Published in final edited form as:

Sci Transl Med. 2019 November 27; 11(520): . doi:10.1126/scitranslmed.aaw3521.

Distinct cellular roles for PDCD10 define a gut-brain axis in cerebral cavernous malformation

Alan T. Tang[1], **Katie R. Sullivan**[1], **Courtney C. Hong**[1], **Lauren M. Goddard**[1], **Aparna Mahadevan**[1], **Aileen Ren**[1], **Heidy Pardo**[2], **Amy Peiper**[2], **Erin Griffin**[2], **Ceylan Tanes**[3], **Lisa M. Mattei**[3], **Jisheng Yang**[1], **Li Li**[1], **Patricia Mericko-Ishizuka**[1], **Le Shen**[4], **Nicholas Hobson**[4], **Romuald Girard**[4], **Rhonda Lightle**[4], **Thomas Moore**[4], **Robert Shenkar**[4], **Sean P. Polster**[4], **Claudia J. Roedel**[5], **Ning Li**[6], **Qin Zhu**[7], **Kevin J. Whitehead**[8], **Xiangjian Zheng**[9,10], **Amy Akers**[11], **Leslie Morrison**[12], **Helen Kim**[13], **Kyle Bittinger**[3], **Christopher J. Lengner**[6,14,15], **Markus Schwaninger**[16], **Anna Velcich**[17], **Leonard Augenlicht**[17], **Salim Abdelilah-Seyfried**[5,18], **Wang Min**[19], **Douglas A. Marchuk**[2], **Issam A. Awad**[4], **Mark L. Kahn**[1,*]

[1]Department of Medicine and Cardiovascular Institute, University of Pennsylvania, 3400 Civic Center Blvd, Philadelphia, Pennsylvania 19104, USA

[2]Department of Molecular Genetics and Microbiology, Duke University School of Medicine, Durham, North Carolina 27710, USA

[3]Division of Gastroenterology, Hepatology, and Nutrition, The Children's Hospital of Philadelphia, Philadelphia, Pennsylvania, 19104, USA

[4]Neurovascular Surgery Program, Section of Neurosurgery, Department of Surgery, The University of Chicago School of Medicine and Biological Sciences, Chicago, Illinois 60637, USA

[5]Institute for Biochemistry and Biologie, Department of Animal Physiology, Potsdam University, Karl-Liebknecht-Str. 24-25, Haus 26, 14476 Potsdam, Germany

[6]Department of Biomedical Sciences, School of Veterinary Medicine, University of Pennsylvania, Philadelphia, PA 19104, USA

[7]Graduate Group in Genomics and Computational Biology, Perelman School of Medicine, University of Pennsylvania, Philadelphia, PA 19104, USA

[8]Division of Cardiovascular Medicine and the Program in Molecular Medicine, University of Utah, Salt Lake City, UT 84112, USA

---

[*]Correspondence should be addressed to: M.L.K. (markkahn@pennmedicine.upenn.edu) Telephone: 215-898-9007 FAX: 215-573-2094.

Author Contributions: AT designed and performed most of the experiments and wrote the manuscript. KS, CH, LG, AM, and AR assisted in experiments. JY and LL performed histologic analysis. RG, TM, RL, NH, RS, LS, SP, and IA performed microCT CCM lesion imaging and quantification in a blinded manner. HP, AP, EG, and DM performed experiments with the adult CCM model. CT, LM, and KB performed 16S sequencing and bioinformatics analysis on the mouse and human microbiome samples. CR and SAS performed zebrafish studies. AT, PM, AA, HK, LM, and IA organized and performed the CCM patient microbiome study. KW, XZ, AV, LA, MS and WM provided critical reagents. NL, QZ, and CL performed single-cell sequencing experiments. MK designed experiments and wrote the manuscript.

Competing interests: The authors declare no competing financial interests. IA is Chairman of the Scientific Advisory Board for Angioma Alliance and provides expert opinions related to clinical care of cerebral cavernous malformations.

Data and materials availability: All data and reagents will be made available upon reasonable request. Transgenic mouse lines not available through public repositories are available from Mark Kahn under a material transfer agreement with the University of Pennsylvania.

[9]Department of Pharmacology, School of Basic Medical Sciences, Tianjian Medical University, China 300070

[10]Centenary Institute, Sydney Medical School, University of Sydney, Sydney, NSW 2050, Australia.

[11]Angioma Alliance, Norfolk, VA 23517, USA

[12]Department of Neurology and Pediatrics, University of New Mexico, Albuquerque, New Mexico 87106, USA

[13]Center for Cerebrovascular Research, Department of Anesthesia and Perioperative Care, University of California San Francisco, San Francisco, California 94110, USA

[14]Department of Cell and Developmental Biology, Perelman School of Medicine, University of Pennsylvania, Philadelphia, PA 19104, USA

[15]Institute for Regenerative Medicine, University of Pennsylvania, Philadelphia, PA 19104, USA.

[16]Institute of Experimental and Clinical Pharmacology and Toxicology, University of Lübeck, 23562 Lübeck, Germany

[17]Department of Cell Biology, Albert Einstein College of Medicine/Albert Einstein Cancer Center, NY, USA

[18]Institute of Molecular Biology, Hannover Medical School, Carl-Neuberg Str. 1, D-30625 Hannover, Germany

[19]Department of Pathology and the Vascular Biology and Therapeutics Program, Yale University School of Medicine, New Haven, Connecticut, USA.

Abstract

Cerebral cavernous malformation (CCM) is a genetic, cerebrovascular disease. Familial CCM is caused by genetic mutations in *KRIT1*, *CCM2* or *PDCD10*. Notably, disease onset is earlier and more severe in individuals with *PDCD10* mutations. Recent studies have shown that lesions arise from excess Mitogen-Activated Protein Kinase Kinase Kinase 3 (MEKK3) signaling downstream of Toll-like Receptor 4 (TLR4) stimulation by lipopolysaccharide (LPS) derived from the gut microbiome. These findings suggest a gut-brain CCM disease axis but fail to define it or explain the poor prognosis of patients with *PDCD10* mutations. Here, we demonstrate that the gut barrier is a primary determinant of CCM disease course, independent of microbiome configuration, that explains the increased severity of CCM disease associated with PDCD10 deficiency. Chemical disruption of the gut barrier with dextran sodium sulfate augments CCM formation in a mouse model, as does genetic loss of *Pdcd10*, but not *Krit1*, in gut epithelial cells. Loss of gut epithelial *Pdcd10* results in disruption of the colonic mucosal barrier. Accordingly, loss of Mucin-2 or exposure to dietary emulsifiers that reduce the mucus barrier increase CCM burden analogous to loss of *Pdcd10* in gut epithelium. Finally, we show that treatment with dexamethasone potently inhibits CCM formation in mice due to the combined effect of action at both brain endothelial cells and gut epithelial cells. These studies define a gut-brain disease axis in an experimental model of CCM in which a single gene is required for two critical components: gut epithelial function and brain endothelial signaling.

One Sentence Summary:

Loss of PDCD10 signaling in brain endothelium and gut epithelium contribute to cerebral cavernous malformation in a mouse model.

Introduction

A gut-brain axis has been implicated in a large number of diseases, including stroke(1, 2), dementia(3), Parkinson's disease(4), metabolic disorders such as diabetes(5, 6) and gastrointestinal diseases such as inflammatory bowel disease(7). Such pathogenic circuits hold the promise of treating diseases in relatively inaccessible sites such as the brain through manipulation of more accessible sites such as the gut or combining gut and brain targets for more effective therapies, but such translation requires clear definition of the pathway between organs. Numerous mechanisms have been proposed to explain connections between the gut and brain, including microbiota-generated metabolites that impact brain function, effects of the gut microbiome on local immune cells that may then travel to the brain, and direct communication between the gut and brain mediated by the nervous system or circulating factors (reviewed in(8–10)). However, for most of these diseases, a clear molecular and cellular basis for a gut-brain axis remains elusive due to the difficulty of demonstrating cause and effect between events occurring at two different sites. Leveraging the discovery of gut-brain disease axes to new therapies requires a better understanding of such relationships.

Cerebral cavernous malformation (CCM) is a vascular disease that predominantly affects the brain and is a common cause of hemorrhagic stroke and seizure(11). Standard of care remains symptom management and neurosurgical resection—there remains no disease-modifying medical therapy(12). CCMs arise due to loss of function mutations in three genes, *KRIT1* (aka *CCM1*), *CCM2*, and *PDCD10* (aka *CCM3*), that encode components of a single, heterotrimeric, adaptor protein complex. This "CCM complex" binds and negatively regulates the Mitogen-Activated Protein Kinase Kinase Kinase 3 (MEKK3 aka MAP3K3) in endothelial cells through a direct interaction between CCM2 and MEKK3(13–17). Familial CCM disease arises due to germline, heterozygous loss of function mutations in any of the three CCM genes, but clinical studies have demonstrated that individuals with *PDCD10* mutations develop disease decades earlier than those with *KRIT1* or *CCM2* mutations and are more likely to suffer disabling brain hemorrhage and stroke(18, 19). Unexpectedly, recent studies demonstrate that lipopolysaccharide (LPS) derived from gram negative bacteria (GNB) in the gut microbiome drives CCM disease by activating Toll-like Receptor 4 (TLR4) and MEKK3 signaling in brain endothelial cells(20). These findings support a gut-brain axis in CCM disease, but it remains unclear how LPS from the gut lumen reaches TLR4 receptors in the brain vasculature and which steps in this journey control pathogenesis.

In the present study, we identify the gut barrier as a critical component of the CCM gut-brain axis that bridges the intestinal microbiome and the brain endothelium during disease pathogenesis. We demonstrate that PDCD10-dependent changes in the colonic gut barrier underlie the clinical observation that germline heterozygosity of *PDCD10* confers a more severe form of CCM disease than germline heterozygosity of *KRIT1* or *CCM2*. We also find that chronic oral intake of P80, a dietary emulsifier present in preserved foods, disrupts the mucus barrier and accelerates CCM formation in a pre-clinical mouse disease model without altering the gut microbiome. Finally, we demonstrate that dexamethasone potently blocks CCM formation in mice due to dual effects in brain endothelial cells and gut epithelial cells, highlighting the translational value of defining a gut-brain disease axis at the molecular and cellular levels.

Results

CCM disease genes are not distinguished by their effects on mouse brain endothelial cell signaling or the human gut microbiome.

CCMs arise due to loss of negative regulation of MEKK3 signaling in brain endothelial cells (compartment #1 in Fig. S1A and (21)). We have recently demonstrated that MEKK3 signaling in brain endothelial cells is stimulated by TLR4 receptors that respond to LPS derived from GNB in the gut microbiome (compartment #2 in Fig. S1A and (20)), predicting that LPS must cross the gut barrier and enter the blood to drive CCM formation (compartment #3 in Fig. S1A). Clinical studies have revealed that CCM disease associated with mutations in *PDCD10* presents decades earlier than that associated with *KRIT1* or *CCM2* mutations, and is associated with larger lesions and greater incidence of symptomatic cerebral hemorrhage(18, 19), an observation not explained by known protein-specific differences in CCM complex function or regulation of the gut microbiome (14, 15, 22, 23). To determine why *PDCD10* familial disease is particularly severe, we first tested whether the requirement for PDCD10 differs from those of KRIT1 or CCM2 at the levels of brain endothelial MEKK3 signaling or the gut microbiome.

To study CCM formation in vivo, we utilized an established neonatal mouse model that entails brain endothelial cell-specific deletion of *Pdcd10* using the *Slco1c1(BAC)-CreERT2* (iBECre;*Pdcd10*$^{fl/fl}$, “inducible brain endothelial Cre”) one day after birth (P1) (Fig. S1B) (24). iBECre;*Pdcd10*$^{fl/fl}$ mice exhibited CCM lesions with gain of endothelial KLF4 expression, a downstream hallmark of elevated endothelial MEKK3 signaling that we, and others, have previously identified in *Krit1* and *Ccm2* mouse-lesions and human CCMs(13, 25, 26) (Fig. S1C–H). Similar to analogous genetic rescue experiments using *Krit1* and *Ccm2* animals, haploinsufficiency of MEKK3 in *Pdcd10* littermates resulted in an eighty percent reduction in lesion volume at P10 assessed visually and through blinded X-ray micro computed tomography (microCT) imaging of the entire mouse brain (Fig. 1A–B)(23, 27, 28). These results indicate that the role of PDCD10 in regulation of endothelial MEKK3 signaling is similar in magnitude to those of KRIT1 and CCM2 and suggest that the basis for more severe PDCD10-associated disease is likely to be an unidentified role for PDCD10 in other cell types or the gut microbiome.

Using the neonatal mouse CCM model, we recently demonstrated that the composition of the gut microbiome plays a vital role in lesion formation, with animals harboring greater numbers of GNB in the colon exhibiting greater CCM lesion formation (Fig. S1A, compartment #2)(20). To test whether patients with *PDCD10*-mediated CCM might exhibit more aggressive disease due to PDCD10 associated changes in the microbiome, we performed 16S rRNA gene sequencing of bacterial DNA extracted from the feces of seventy-five genotyped CCM patients with detectable lesions using magnetic resonance imaging (MRI) and compared these samples to twenty-nine healthy volunteers from multiple clinical sites in the United States (Table S1)(29). A PERMANOVA test on weighted UniFrac distances revealed a significant ($p=0.002$) separation of the microbiome communities in patients with CCM disease and those in control individuals (Fig. 1C). Fitting linear models for logit transformed relative abundances of commonly present bacterial taxa revealed that gram negative *Bacteroides* were more abundant in individuals with CCM disease than in controls (Fig. 1D), while gram positive *Lachnospiraceae* were less abundant (Fig. S1I). Individuals with familial *PDCD10* disease did not exhibit microbiomes different from those with familial *KRIT1* or *CCM2* disease, either globally (Fig. 1E) or with respect to changes in gram negative *Bacteroides* or gram positive *Lachnospiraceae* species (Fig. 1F and S1J). Although conclusions drawn from these data are limited by the relatively small sample size and biased towards symptomatic CCM disease, they support the concept that environmental factors dominate over host genetics to alter gut microbial ecology(30). Taken together, our mouse genetic and human microbiome studies suggest that the basis for a more aggressive clinical course in familial *PDCD10* disease is neither a unique signaling role in brain endothelial cells nor a specific effect on the gut microbiome, and therefore might reflect a previously unrecognized role for PDCD10 in the intervening gut barrier.

Chemical disruption of the gut barrier accelerates CCM formation in mice

To test whether disruption of the gut barrier worsens CCM disease, we combined the dextran-sodium sulfate (DSS) colitis and neonatal CCM mouse models. As previously described(13), to initiate the neonatal CCM model we induced endothelial cell-specific deletion of *Krit1* one day after birth (P1) using the *Cdh5(PAC)-CreERT2* (iECre;*Krit1*$^{fl/fl}$, “inducible endothelial Cre”). Starting at P10, 2.5% DSS was orally administered once daily for five days, resulting in varying degrees of colitis ranging from epithelial thickening and crypt abscesses to complete erosion of the colonic epithelium at P21, with colitis observed in 5 animals treated with DSS and no colitis in 4 controls (Fig. 2A–B, $p<0.05$). Approximately fifty percent of neonatal animals administered DSS did not survive to P21 (likely a result of DSS effects and lethality associated with gavaging neonatal mice), but survivors (20 of 45 total animals) exhibited an approximate two-fold increase in CCM volume compared to littermate, vehicle-treated animals (Fig. 2C–D).

We previously characterized distinct *Krit1* and *Ccm2* mouse colonies that are respectively resistant and susceptible to CCM formation due to qualitative differences in the gut microbiome(20). Susceptible, vehicle-treated iECre;*Krit1*$^{fl/fl}$ animals spontaneously developed appreciable lesion volume (Fig. 2C–D), whereas resistant, vehicle-treated iECre;*Ccm2*$^{fl/fl}$ animals exhibited barely detectable lesions (Fig. 2E–F). Analogous to the *Krit1* experiments performed in susceptible animals, resistant, DSS-treated iECre;*Ccm2*$^{fl/fl}$ animals exhibited a ten-fold increase in lesion volume (Fig. 2E–F). These results demonstrate that broad disruption of the colonic epithelium exacerbates CCM disease in a manner independent of genotype or baseline microbiome.

Gut epithelial loss of PDCD10 but not KRIT1 accelerates CCM lesion formation.

The exacerbation of CCM formation by DSS treatment identified the gut barrier as a potentially rate-limiting mechanism of disease pathogenesis. Although the gut barrier is a complex, multi-cellular system, its primary component is the gut epithelium. Analysis of single-cell gene expression in intestinal epithelial cells (IECs) revealed broad transcription of *Krit1, Ccm2*, and *Pdcd10* across cell-types (Fig. S2). We therefore hypothesized that PDCD10 might play a role in gut barrier integrity distinct from that of KRIT1 and CCM2. To study the role of IEC PDCD10 in the context of CCM disease, we compared CCM formation in animals with both inducible brain endothelial cell deletion (iBECre) at P1 and constitutive IEC deletion (Villin1-Cre, "VilCre") of *Pdcd10* (iBECre;VilCre;*Pdcd10*$^{fl/fl}$), to littermates with only inducible brain endothelial cell deletion of *Pdcd10* (iBECre;*Pdcd10*$^{fl/fl}$). Loss of IEC *Pdcd10* resulted in a twofold increase in lesion burden by P21 (Fig. 3A–B). To determine if PDCD10 plays a specific role in IECs during CCM formation relative to the other CCM genes, we performed the analogous *Krit1* experiment. Loss of IEC *Krit1* had no effect on lesion formation (Fig. 3C–D).

A notable clinical aspect of familial *PDCD10* disease is the high rate of cerebral hemorrhage compared with familial *KRIT1* or *CCM2* disease(19). Histologic examination of iBECre;VilCre;*Pdcd10*$^{fl/fl}$ mouse brains at P21 revealed both large CCM lesions in the white matter of the cerebellum as well as numerous sites of peri-lesional hemorrhage (Fig. 3E and S3A). Although large, multi-cavernous lesions were also observed in iBECre;*Pdcd10*$^{fl/fl}$ brains, following deletion of *Pdcd10* solely in brain endothelium (Fig. 3F and S3A), no peri-lesional hemorrhage was observed, consistent with prior studies of the neonatal CCM model(31). Hemorrhage was not observed in either animals with loss of only a single *Pdcd10* allele in brain endothelium and IECs, animals with complete loss of *Pdcd10* only in IECs (Fig. 3G and Fig. S3B–E), or in either iECre;VilCre;*Krit1*$^{fl/fl}$ or iECre;*Krit1*$^{fl/fl}$ mouse brains at P21 (Fig. 3H–I and S3A). These findings identify a role for PDCD10 in the gut epithelium during CCM formation in mice distinct from that of KRIT1.

Loss of gut epithelial PDCD10 but not KRIT1, CCM2 or MEKK3 results in loss of the colonic mucus layer

Since most gram-negative bacteria and GNB-derived LPS reside in the colon, to understand the role of PDCD10 in IECs during CCM formation we analyzed the colons of the same iBECre;*Pdcd10*$^{fl/fl}$ and iBECre;VilCre;*Pdcd10*$^{fl/fl}$ animals presented in Figure 3 (Fig. 4A). Since individuals with familial *PDCD10* disease are germline heterozygous, we also analyzed colons from littermate iBECre;VilCre;*Pdcd10*$^{fl/+}$ animals (Fig. 4A, middle). A major component of the colonic gut barrier is the mucus layer, produced by goblet cells, that physically separates gut bacteria from gut epithelium(32), and an initial event in DSS-associated colitis is disruption of the mucus barrier (33). Analysis of the colonic mucus barrier using methacarn-fixed samples (Fig. S4 and (32, 34)) revealed a significant ($p<0.0001$) reduction of the mucus layer following homozygous or heterozygous loss of IEC *Pdcd10* at P21 (Fig. 4A and C). In contrast, loss of IEC *Krit1, Ccm2*, or *Map3k3* had no effect on mucus layer dimensions at P21 (Fig. 4B and D, S5, S6). Additionally, loss of IEC PDCD10 was associated with markedly swollen goblet cells (Fig. 4A and S7A), but no change in the expression of *Muc2* mRNA or MUC2 protein (Fig. S7C–F), whereas loss of IEC *Krit1* was not associated with any change in goblet cell vesicle size (Fig. 4B and S7B).

VilCre;*Pdcd10*$^{fl/+}$ and VilCre;*Pdcd10*$^{fl/fl}$ animals exhibited increased concentration of fecal lipocalin-2 (LCN2, aka NGAL), a secreted inflammatory-response protein that has been shown to be a sensitive and dynamic marker of colitis (Fig. 4E)(35) that was not observed following IEC loss of *Krit1, Ccm2 or Map3k3* (Fig. 4F, S5, S6). Consistent with the rise in fecal LCN2, P21 iBECre;VilCre;*Pdcd10*$^{fl/+}$ and iBECre;VilCre;*Pdcd10*$^{fl/fl}$ colons exhibited crypt dilation, an early sign of inflammation (Fig. 4A and S7G), and crypt abscesses marked by Ly6G-positive neutrophils (Fig. 4G and I). In contrast, P21 iECre;VilCre;*Krit1*$^{fl/fl}$ animals exhibited normal colonic crypts without crypt abscesses (Fig. 4B, H, J and S7H).

Our prior studies have demonstrated that the amount of circulating LPS determines CCM formation in mouse models, suggesting that loss of gut barrier function associated with IEC PDCD10 deficiency might augment CCM formation by permitting more translocation of GNB-derived LPS from the gut lumen to the circulating blood(20). Consistent with such a mechanism, loss of IEC PDCD10 resulted in elevated TLR4-agonist activity in circulating blood from P21 animals (Fig. 4K). In contrast, loss of IEC KRIT1 had no effect on TLR4-agonist activity in circulating blood from P21 animals (Fig. 4L). An increase in blood TLR4 activation was not detected in animals with heterozygous loss of IEC *Pdcd10* (iBECre;VilCre;*Pdcd10*$^{fl/+}$), most likely due to a low basal rate of leak/translocation and the limited sensitivity of measuring circulating LPS at a single-timepoint compared with growth of CCM lesions over 21 days (Fig. 4K).

Genetic loss of colonic mucus accelerates CCM formation in mice.

The studies described above suggested that a primary mechanism by which PDCD10 deficiency in IECs might accelerate CCM formation is through loss of the mucus layer that prevents GNB from reaching the gut wall and translocating to the blood(32–34, 36–38). To directly test the role of the mucus layer in CCM formation, we examined the effect of loss of Mucin-2 (MUC2), a glycoprotein secreted by goblet cells that is the primary constituent of the colonic mucosal barrier(34, 38), on lesion formation following *Pdcd10* gene deletion in brain endothelial cells at P1. Loss of one or two *Muc2* alleles conferred a dose-dependent decrease in both the mucus layer and CCM lesion volume of P21 animals like those observed following loss of one or two *Pdcd10* alleles in IECs (Fig. 5A–D).

The CCM proteins, particularly KRIT1, have been implicated in the maintenance of endothelial junctions and epithelial junction integrity is another component of the gut barrier underlying colonic mucus(39, 40). Loss of gut epithelial PDCD10 resulted in decreased E-cadherin (CDH1) but increased EpCAM (EPCAM) junction continuity and no changes in F-actin or ZO-1, whereas loss of gut epithelial KRIT1 did not affect junctions (Fig. S8A–D, S9A–D, and S10). *Muc2* null colons exhibited decreased E-cadherin and EpCAM junction continuity, but *Muc2* heterozygous colonic epithelial junctions were unchanged (Fig. S8E–F and S9E–F). Thus, *Muc2* heterozygosity worsens CCM burden in the setting of a decreased colonic mucus barrier but unchanged epithelial junctions. Overall, these findings suggest that a primary mechanism by which *Pdcd10* prevents CCM formation in IECs is through its role in maintaining the colonic mucus layer.

The gut barrier can regulate CCM formation independent of the gut microbiome.

In addition to providing a protective layer for the intestinal epithelium, the abundant glycoprotein MUC2 serves as a food source for luminal bacteria and affects microbial ecology(41). Moreover, MUC2 secretion by goblet cells is bacterial-ligand dependent and affected by qualitative differences in the gut microbiome(37, 42). Thus, changes in mucus expression could affect CCM formation through changes in the gut microbiome as well as the gut barrier. To address the relationship between the gut barrier and the gut microbiome, we next performed 16S rRNA gene sequencing of bacterial DNA extracted from the feces of mice with genetic loss of epithelial *Pdcd10*, *Krit1*, or *Muc2*. Since cage and litter effects are a confounding factor in gut microbiome studies(43), we collected fecal pellets from P21 animals prior to weaning when the entire litter remained co-housed (Fig. 6A), and all analyses were performed considering individual cage effects (Fig. S11). A PERMANOVA test of unweighted UniFrac distances revealed a separation of bacterial microbiome communities from VilCre;*Pdcd10*$^{fl/fl}$ mice compared with either VilCre;*Pdcd10*$^{fl/+}$ or *Pdcd10*$^{fl/fl}$ littermates (Fig. 6B and Fig. S11A, and Fig. S12A). A similar separation was observed when iBECre;VilCre;*Pdcd10*$^{fl/fl}$ animals were compared with iBECre;VilCre;*Pdcd10*$^{fl/+}$ or iBECre;*Pdcd10*$^{fl/fl}$ littermates (Fig. 6C and Fig S11B and Fig. S12B). A significant ($p<0.001$) separation of bacterial microbiome communities was also observed between iBECre;*Pdcd10*$^{fl/fl}$;*Muc2*$^{-/-}$ when compared to either iBECre;*Pdcd10*$^{fl/fl}$;*Muc2*$^{+/-}$ or iBECre;*Pdcd10*$^{fl/fl}$;*Muc2*$^{+/+}$ littermates (Fig. 6D and Fig. S11C and Fig. S12C). In contrast, no significant ($p=0.311$) separation of bacterial microbiome communities was observed between *Krit1*$^{fl/fl}$ and VilCre;*Krit1*$^{fl/fl}$ animals (Fig. 6E and Fig. S11D and Fig. S12D). Fitting generalized, linear mixed effects models for logit transformed relative abundances of commonly present bacterial taxa identified almost identical shifts for VilCre;*Pdcd10*$^{fl/fl}$, iBECre;VilCre;*Pdcd10*$^{fl/fl}$ and iBECre;*Pdcd10*$^{fl/fl}$;*Muc2*$^{-/-}$ animals, including a significant ($q\leq0.05$) increase in *Bacteroides, Rikenellaceae* and decrease in *s24–7*, *Prevotellaceae* and *Alloprevotella* species (Fig. 6F and Fig. S13). The observation that loss of gut epithelial *Pdcd10* conferred biome changes indistinguishable from those associated with loss of *Muc2* provides additional evidence that a major effect of IEC PDCD10 loss is disruption of the colonic mucosal barrier comprised of MUC2. Importantly, analysis of heterozygous VilCre;*Pdcd10*$^{fl/+}$, iBECre;VilCre;*Pdcd10*$^{fl/+}$ and iBECre;*Pdcd10*$^{fl/fl}$;*Muc2*$^{+/-}$ animals revealed no significant ($q>0.05$) changes in the gut microbiome (Fig. 6G), even though iBECre;*Pdcd10*$^{fl/fl}$;*Muc2*$^{+/-}$ animals exhibited increased CCM formation. These findings support the conclusion that changes in gut barrier may influence CCM formation independent of changes in the gut microbiome.

The dietary emulsifier P80 degrades colonic mucus and accelerates CCM formation in mice.

The studies of DSS exposure and IEC loss of PDCD10 and MUC2 described above suggested that dietary agents that reduce the colonic mucosal barrier may accelerate CCM disease. A recent study reported that dietary emulsifiers, like those commonly found in processed foods, promote colitis by degrading the colonic mucosal barrier(44). To test whether ingestion of a common dietary emulsifier might drive CCM formation through changes in the gut barrier, we first exposed *Pdcd10*$^{+/-}$ animals to oral 1% P80 emulsifier for two weeks and assessed the thickness of the colonic mucus layer. P80 emulsifier exposure resulted in a fifty percent reduction in the mucus layer (Fig 7A, B). 16S rRNA gene sequencing of bacterial DNA extracted from the feces of *Pdcd10*$^{+/-}$ mice treated with P80 or vehicle alone revealed that chronic emulsifier exposure did not result in a significant ($p>0.05$) separation of bacterial microbiome communities when accounting for cage effects (Fig. 7C, D and Fig. S14). We next assessed whether chronic exposure to DSS could affect CCM formation. Although aged *Krit1*$^{+/-}$ animals exhibited no detectable lesion formation after 6 months (Fig. 7E and G), aged *Pdcd10*$^{+/-}$ animals exhibited a low but significant ($p<0.01$) rate of spontaneous lesion formation (Fig. 7F–G). Chronic treatment of *Pdcd10*$^{+/-}$ animals with 1% P80 significantly ($p<0.05$) increased lesion formation (Fig. 7F–G). These studies suggest that emulsifiers commonly found in preserved or processed foods may exacerbate CCM formation through effects on the gut mucosal barrier that are independent of the gut microbiome.

Dexamethasone potently inhibits CCM formation through dual effects on brain endothelial cells and gut epithelial cells.

The studies described above and our prior studies(20) identify a gut-brain CCM disease axis in which PDCD10 functions in both IECs and brain endothelial cells to control the movement of LPS from the gut lumen into the blood and the response to blood-borne LPS in the brain. This model predicts that therapies able to simultaneously increase gut barrier function by IECs and reduce TLR4-MEKK3-KLF2/4 signaling by brain ECs might potently inhibit CCM formation. Glucocorticoids confer pleiotropic cell and organ effects that are primarily mediated by gene expression changes downstream of glucocorticoid receptor NR3C1 (GR) signaling(45). Loss of GR function confers increased responses to LPS in endothelial cells(46, 47), while the glucocorticoid dexamethasone increases MUC2 expression by IECs (48). suggesting that dexamethasone, a highly selective GR agonist(49), might act at both ends of the CCM gut-brain disease axis to prevent lesion formation.

A single dose of dexamethasone administered at P5 entirely blocked CCM formation in both iECre;*Krit1*$^{fl/fl}$ and iECre;*Pdcd10*$^{fl/fl}$ neonates (Fig. 8A–C and Fig. S15A–E). The effect of dexamethasone blocked lesion formation using a single doses as low as 0.4 mg/kg (Fig. 8A), less than that commonly administered for asthma exacerbations in human patients. Analysis of brain endothelial gene expression revealed marked reductions in the mRNA transcripts of *Map3k3* (*Mekk3*) as well as the downstream MEKK3 targets *Klf2* and *Klf4* and the upstream MEKK3 activators *Tlr4* and *Cd14* following dexamethasone administration (Fig. 8D).

To test whether rescue was mediated by changes in brain endothelial cells, the effect of dexamethasone was examined in iECre;*Krit1*$^{fl/fl}$;*Nr3c1*$^{fl/fl}$ animals in which endothelial loss of KRIT1 is accompanied by endothelial loss of GR. Dexamethasone treatment continued to potently prevent lesion formation in iECre;*Krit1*$^{fl/fl}$;*Nr3c1*$^{fl/fl}$ animals (Fig. 8E–F), indicating that the effect of dexamethasone was not merely due to effects in brain endothelial cells. Analysis of the intestine of dexamethasone-treated animals revealed marked colonic dilatation (Fig. S15E) that was accompanied by a large increase in goblet cell activity and MUC2 production (Fig. 8GH and S15F–H). The increase in mucus production stimulated by dexamethasone was ablated in VilCre;*Nr3c1*$^{\mathrm{fl/fl}}$ animals (Fig. S15I–J), indicating that it is mediated by stimulation of IEC GR. To test whether dexamethasone rescue of CCM formation is mediated primarily by effects on IEC mucus production, we examined rescue in mice lacking MUC2. Dexamethasone potently prevented lesion formation in iBECre;*Pdcd10*$^{\mathrm{fl/fl}}$;*Muc2*$^{-/-}$ animals (Fig. 8I–K), indicating that rescue was also not merely due to effects on IECs. To test whether the potent dexamethasone effect was due to dual action in both brain endothelial cells and IECs, we next examined dexamethasone rescue in iECre;*Krit1*$^{\mathrm{fl/fl}}$;*Nr3c1*$^{\mathrm{fl/fl}}$ animals lacking GR only in endothelial cells and in littermate iECre;VilCre;*Krit1*$^{\mathrm{fl/fl}}$;*Nr3c1*$^{\mathrm{fl/fl}}$ animals lacking GR in both endothelial cells and IECs. iECre;*Krit1*$^{\mathrm{fl/fl}}$;*Nr3c1*$^{\mathrm{fl/fl}}$ animals treated with dexamethasone failed to develop CCMs (Fig. 8L), but dexamethasone-treated iECre;VilCre;*Krit1*$^{\mathrm{fl/fl}}$;*Nr3c1*$^{\mathrm{fl/fl}}$ animals developed robust lesion formation like those given vehicle only (Fig. 8M–N). Although we cannot exclude effects of dexamethasone on the gut microbiome, effects of dexamethasone on other cell types such as immune cells, or the possibility that rescue is mediated solely by GR signaling in IECs, the potent ability of dexamethasone to block CCM formation is most readily explained by dual effects on brain endothelial cell signaling and IEC gut barrier formation. These studies suggest that pharmacologic targeting of multiple sites in a gut-brain axis disease mechanism may yield powerful therapeutic strategies (Fig. S15K–L).

Discussion

A central molecular component of the gut-brain axis in CCM disease identified by these studies is the colonic mucus barrier that physically separates GNB in the colon from the epithelial cell layer and underlying blood vessels of the host. Loss of *Pdcd10* in gut epithelial cells resulted in a dose-dependent reduction in the thickness of the colonic mucus layer that correlated with an increase in CCM lesion formation. The changes in mucus layer thickness and CCM formation conferred by loss of IEC *Pdcd10* were replicated by dose-dependent loss of *Muc2*. A causal relationship between IEC *Pdcd10* and formation of the mucus barrier was further supported by nearly identical changes in gut microbial taxa abundance observed upon loss of *Pdcd10* or *Muc2*. These findings suggested that PDCD10 regulation of mucus production by goblet cells was a likely mechanism for its role in gut epithelial cells in CCM disease. Histologic analysis of the VilCre;*Pdcd10*$^{\mathrm{fl/fl}}$ colon revealed abnormal, swollen goblet cells that contained large amounts of mucin despite the loss of the extra-epithelial mucus barrier. Moreover, qPCR and western blot analysis of colonic epithelium demonstrated preserved total MUC2 mRNA and protein content in the colons of VilCre;*Pdcd10*$^{\mathrm{fl/+}}$ and VilCre;*Pdcd10*$^{\mathrm{fl/fl}}$ animals. Taken together, these findings are consistent with a requirement for PDCD10 during mucus secretion rather than MUC2 expression.

Our findings provide an explanation for the clinical observation that germline haploinsufficiency of *PDCD10* confers a more aggressive disease phenotype than germline haploinsufficiency of *KRIT1* or *CCM2*. Furthermore, they suggest that PDCD10 functions independently of the CCM complex in gut epithelial cells. Consistent with this observation, we found that gut epithelial loss of MEKK3, the kinase regulated by the CCM complex to prevent CCM formation by brain endothelial cells, also does not result in any change in the gut barrier. How does PDCD10 function to regulate the gut barrier? PDCD10 is a component of Striatin-interacting phosphatase and kinase (STRIPAK) complexes that do not include KRIT1 or CCM2 and are not known to target MEKK3(50). Moreover, PDCD10 has recently been found to participate in vesicle exocytosis in mammalian cells(51, 52) and vesicle trafficking in *C. elegans*(53). Thus, although future studies are required to fully define the role of PDCD10 in gut epithelial cells, a mechanism in which PDCD10 functions as part of the STRIPAK but not CCM complex to regulate mucin secretion by goblet cells seems likely.

We acknowledge three main limitations regarding these findings. First, we cannot exclude the possibility that unique PDCD10 signaling in endothelial cells contributes to increased disease severity, although we demonstrated that the primary mechanism of lesion formation is gain of brain endothelial MEKK3 signaling(52). Second, although we showed in a variety of contexts that the gut barrier can affect CCM severity independently of the gut microbiome, these entities are so complex and intertwined that precisely parsing their individual effects is difficult. Third, this study was performed in mouse models; therefore, translation to human disease remains unproven. Our study illustrates the need to consider both the gut microbiome and barrier when assessing CCM disease risk in patients.

Can our findings can be translated to improve the treatment and management of CCM patients? First, proposed pharmacologic therapies for CCM disease must consider potential effects on gut barrier function. Drugs that adversely affect the gut barrier would be contraindicated, particularly as a chronic, lifelong therapy. Second, our studies of *Pdcd10*$^{+/-}$ animals with oral P80 intake confirm prior reports that such agents can reduce the colonic mucus barrier and suggest that common dietary factors such as emulsifiers in processed foods may have a relevant impact on CCM disease course through deleterious effects on the gut barrier. Third, exacerbation of CCM formation by DSS, commonly used to model inflammatory bowel disease in mice, suggests that gastrointestinal conditions associated with chronic inflammation, such as inflammatory bowel disease, are likely to accelerate CCM formation through effects on the gut barrier. Conversely, conditions that increase mucus production and/or reduce gut inflammation would be predicted to slow CCM disease progression.

Finally, defining a gut-brain disease axis at the molecular and cellular levels enables the design of therapies to treat diseases refractory to conventional, “on-site” strategies. We have modeled such a therapeutic approach through analysis of an unexpectedly potent glucocorticoid treatment for CCM disease in mice. Genetic dissection of the dexamethasone mechanism of action to prevent CCM formation revealed that the drug acted through GRs in two cell types: brain endothelium and gut epithelium. Thus, the basis for dexamethasone’s potency was most likely the fact that it targeted multiple key molecular and cellular mechanisms in the CCM gut-brain axis. Analogous single or multiple drug strategies designed to disable well-defined gut-brain axes may yield potent therapeutic strategies for other such pathologies in the future.

Materials and Methods

Study design

As previously described(20), our lab has extensive experience with the P10 neonatal CCM mouse model. Sample sizes were estimated based on our previous experience with the neonatal CCM model and lesion volume quantitation by blinded microCT and our sample size calculations were previously detailed. Briefly, at P10, seven animals in each group would be expected to sufficiently power a study at 80% (β=0.2) at a significance level of α=0.05 assuming an expected effect size of 80%, equal standard deviations, and normal distributions. For the P21 neonatal CCM model, we collected twenty brains at P21 and calculated a mean of 0.4 and standard deviation of 0.2. Based on our initial experience with DSS colitis in Figure 2c–d, we assumed an effect size of 50%. Thus, each group would require 16 animals to power a study at 80% (β=0.2) with a significance level of α=0.05 assuming equal standard deviations and normal distributions. No data inclusion/exclusion or endpoint criteria were pre-defined or applied. No outliers were defined or excluded. Each experiment was performed at least twice with different litters and n greater than or equal to three (see specifics in each figure legend).

Research objectives were to define the role of the gut barrier in CCM severity using genetically engineered mouse models. We hypothesized that defects in the gut barrier would increase disease severity and that the clinical aggressiveness of *PDCD10* familial disease is caused by defects in gut barrier due to a unique role for PDCD10 in the intestinal epithelium. Research subjects included human CCM patients and primarily genetically engineered mouse models. All experimental and control animals were littermates, and none were excluded from analysis at the time of harvest. Experimental animals were lost or excluded at two pre-defined points: (i) failure to properly inject 4OHT and observation of substantial leakage; (ii) death prior to P10 or P21 because of 4OHT injection or drug administration or other unknown causes. Given the early time points prior to weaning or sexual maturity, no attempt was made to distinguish, or segregate results based on gender. Prior studies have found that adult animals heterozygous for CCM genes did not exhibit any difference in lesion burden with respect to gender(54, 55), so no attempt was made to distinguish genders of animals used in adult CCM experiments.

Blinding was performed at multiple points during the experiments. Induction of the neonatal disease model was performed at one day of birth without knowledge of genotypes. MicroCT lesion volume quantification was performed in a blinded manner by investigators without knowledge of experimental details. 16S sequencing of both mouse and human samples were performed in blinded fashion until final analysis.

Statistics

As indicated in the specific figure legends, the standard error of the mean (s.e.m.), 95% confidence interval, or boxplot is shown. Column data for each experiment was subjected to D’Agostino & Pearson normality tests and only the P80 emulsifier experiments did not satisfy this test. We also found that in almost all experiments, the variance between groups was significantly ($p<0.05$) different. Accordingly, we utilized unpaired, two-tailed, Welch’s t-tests for all two-group analyses, Kruskall-Wallis (non-parametric) one-way ANOVA with Dunn's correction for multiple comparisons in multiple-group analyses, or Mann-Whitney non-parametric U-tests for experiments that did not satisfy normality tests. Since the Welch's t-test underperforms on small sample sizes, and variance calculations are meaningless for smaller samples, experiments with groups less than or equal to ten distinct samples were analyzed using the unpaired, two-tailed Student's t-test or one-way ANOVA with Holm-Sidak correction for multiple comparisons. Statistical tests for 16S sequencing analyses are detailed in the prior methods sections and all significance ($p<0.05$ or $q<0.05$) tests were corrected for multiple comparisons using Bonferroni or Benjamini-Hochberg methods.

Supplementary Material

Refer to Web version on PubMed Central for supplementary material.

Acknowledgements:

We thank the members of the Kahn lab; our colleagues Jorge Henao-Mejia, Gary Wu, and Rick Bushman for their thoughtful comments and advice during this work. We thank Angioma Alliance for patient enrollment, the University of Chicago PaleoCT core facilities' expertise, and Lili Guo for artwork.

Funding: Supported by National Institute of Health grants R01HL094326 to MK, P01NS092521 to MK, DM, IA, F30NS100252 to AT, RO1CA174432 to LA, R01CA229216 to LA, R01HL136507 to WM; U54NS065705 to HK, LM; German DFG grant SCHW416/5-2 to MS, SE2016/7-2 and SE2016/10-1 to SAS; National Natural Science Foundation of China grants 81771240 to XZ; Australian National Health and Medical Research Council project grant APP1124011 to XZ; Excellence cluster REBIRTH SFB958 to SAS; a Penn-CHOP Microbiome Pilot & Feasibility Award Grant to MK, and a Be Brave for Life Micro-Grant to MK. Single cell sequencing supported by a grant from the State of Pennsylvania Health Research Formula Fund to CL. MicroCT imaging supported by University of Chicago Safadi Program of Excellence in Clinical and Translational Neuroscience Pilot Awards to LS and SP.

References and Notes:

1. Benakis C, Brea D, Caballero S, Faraco G, Moore J, Murphy M, Sita G, Racchumi G, Ling L, Pamer EG, Iadecola C, Anrather J, Commensal microbiota affects ischemic stroke outcome by regulating intestinal gammadelta T cells. Nat Med 22, 516–523 (2016); published online EpubMay (10.1038/nm.4068). [PubMed: 27019327]
2. Stanley D, Mason LJ, Mackin KE, Srikhanta YN, Lyras D, Prakash MD, Nurgali K, Venegas A, Hill MD, Moore RJ, Wong CH, Translocation and dissemination of commensal bacteria in post-stroke infection. Nat Med 22, 1277–1284 (2016); published online EpubNov (10.1038/nm.4194). [PubMed: 27694934]
3. Faraco G, Brea D, Garcia-Bonilla L, Wang G, Racchumi G, Chang H, Buendia I, Santisteban MM, Segarra SG, Koizumi K, Sugiyama Y, Murphy M, Voss H, Anrather J, Iadecola C, Dietary salt promotes neurovascular and cognitive dysfunction through a gut-initiated TH17 response. Nature neuroscience 21, 240–249 (2018); published online EpubFeb (10.1038/s41593-017-0059-z). [PubMed: 29335605]
4. Sampson TR, Debelius JW, Thron T, Janssen S, Shastri GG, Ilhan ZE, Challis C, Schretter CE, Rocha S, Gradinaru V, Chesselet MF, Keshavarzian A, Shannon KM, Krajmalnik-Brown R, Wittung-Stafshede P, Knight R, Mazmanian SK, Gut Microbiota Regulate Motor Deficits and Neuroinflammation in a Model of Parkinson's Disease. Cell 167, 1469–1480 e1412 (2016); published online EpubDec 01 (10.1016/j.cell.2016.11.018). [PubMed: 27912057]
5. Wang PY, Caspi L, Lam CK, Chari M, Li X, Light PE, Gutierrez-Juarez R, Ang M, Schwartz GJ, Lam TK, Upper intestinal lipids trigger a gut-brain-liver axis to regulate glucose production. Nature

452, 1012–1016 (2008); published online EpubApr 24 (10.1038/nature06852). [PubMed: 18401341]

6. Perry RJ, Peng L, Barry NA, Cline GW, Zhang D, Cardone RL, Petersen KF, Kibbey RG, Goodman AL, Shulman GI, Acetate mediates a microbiome-brain-beta-cell axis to promote metabolic syndrome. Nature 534, 213–217 (2016); published online EpubJun 9 (10.1038/nature18309). [PubMed: 27279214]
7. Bonaz BL, Bernstein CN, Brain-gut interactions in inflammatory bowel disease. Gastroenterology 144, 36–49 (2013); published online EpubJan (10.1053/j.gastro.2012.10.003). [PubMed: 23063970]
8. Sharon G, Garg N, Debelius J, Knight R, Dorrestein PC, Mazmanian SK, Specialized metabolites from the microbiome in health and disease. Cell Metab 20, 719–730 (2014); published online EpubNov 4 (10.1016/j.cmet.2014.10.016). [PubMed: 25440054]
9. Fung TC, Olson CA, Hsiao EY, Interactions between the microbiota, immune and nervous systems in health and disease. Nature neuroscience 20, 145–155 (2017); published online EpubFeb (10.1038/nn.4476). [PubMed: 28092661]
10. Spadoni I, Fornasa G, Rescigno M, Organ-specific protection mediated by cooperation between vascular and epithelial barriers. Nat Rev Immunol 17, 761–773 (2017); published online EpubDec (10.1038/nri.2017.100). [PubMed: 28869253]
11. Spiegler S, Rath M, Paperlein C, Felbor U, Cerebral Cavernous Malformations: An Update on Prevalence, Molecular Genetic Analyses, and Genetic Counselling. Molecular syndromology 9, 60–69 (2018); published online EpubFeb (10.1159/000486292). [PubMed: 29593473]
12. Akers A, Al-Shahi Salman R, Dahlem AAI,K, Flemming K, Hart B, Kim H, Jusue-Torres I, Kondziolka D, Lee C, Morrison L, Rigamonti D, Rebeiz T, Tournier-Lasserve E, Waggoner D, Whitehead K, Synopsis of Guidelines for the Clinical Management of Cerebral Cavernous Malformations: Consensus Recommendations Based on Systematic Literature Review by the Angioma Alliance Scientific Advisory Board Clinical Experts Panel. Neurosurgery 80, 665–680 (2017); published online EpubMay 01 (10.1093/neuros/nyx091). [PubMed: 28387823]
13. Zhou Z, Tang AT, Wong WY, Bamezai S, Goddard LM, Shenkar R, Zhou S, Yang J, Wright AC, Foley M, Arthur JS, Whitehead KJ, Awad IA, Li DY, Zheng X, Kahn ML, Cerebral cavernous malformations arise from endothelial gain of MEKK3-KLF2/4 signalling. Nature 532, 122–126 (2016); published online EpubApr 7 (10.1038/nature17178). [PubMed: 27027284]
14. Fisher OS, Deng H, Liu D, Zhang Y, Wei R, Deng Y, Zhang F, Louvi A, Turk BE, Boggon TJ, Su B, Structure and vascular function of MEKK3-cerebral cavernous malformations 2 complex. Nat Commun 6, 7937 (2015)10.1038/ncomms8937). [PubMed: 26235885]
15. Wang X, Hou Y, Deng K, Zhang Y, Wang DC, Ding J, Structural Insights into the Molecular Recognition between Cerebral Cavernous Malformation 2 and Mitogen-Activated Protein Kinase Kinase Kinase 3. Structure, (2015); published online EpubApr 29 (10.1016/j.str.2015.04.003).
16. Cullere X, Plovie E, Bennett PM, MacRae CA, Mayadas TN, The cerebral cavernous malformation proteins CCM2L and CCM2 prevent the activation of the MAP kinase MEKK3. Proc Natl Acad Sci U S A, (2015); published online EpubNov 4 (10.1073/pnas.1510495112).
17. Zhou Z, Rawnsley DR, Goddard LM, Pan W, Cao XJ, Jakus Z, Zheng H, Yang J, Arthur JS, Whitehead KJ, Li D, Zhou B, Garcia BA, Zheng X, Kahn ML, The cerebral cavernous malformation pathway controls cardiac development via regulation of endocardial MEKK3 signaling and KLF expression. Dev Cell 32, 168–180 (2015); published online EpubJan 26 (10.1016/j.devcel.2014.12.009). [PubMed: 25625206]
18. Denier C, Labauge P, Bergametti F, Marchelli F, Riant F, Arnoult M, Maciazek J, Vicaut E, Brunereau L, Tournier-Lasserve E, Genotype-phenotype correlations in cerebral cavernous malformations patients. Ann Neurol 60, 550–556 (2006); published online EpubNov ([PubMed: 17041941]
19. Shenkar R, Shi C, Rebeiz T, Stockton RA, McDonald DA, Mikati AG, Zhang L, Austin C, Akers AL, Gallione CJ, Rorrer A, Gunel M, Min W, Marcondes de Souza J, Lee C, Marchuk DA, Awad IA, Exceptional aggressiveness of cerebral cavernous malformation disease associated with PDCD10 mutations. Genet Med 17, 188–196 (2015); published online EpubMar (10.1038/gim.2014.97). [PubMed: 25122144]
20. Tang AT, Choi JP, Kotzin JJ, Yang Y, Hong CC, Hobson N, Girard R, Zeineddine HA, Lightle R, Moore T, Cao Y, Shenkar R, Chen M, Mericko P, Yang J, Li L, Tanes C, Kobuley D, Vosa U,

Whitehead KJ, Li DY, Franke L, Hart B, Schwaninger M, Henao-Mejia J, Morrison L, Kim H, Awad IA, Zheng X, Kahn ML, Endothelial TLR4 and the microbiome drive cerebral cavernous malformations. Nature 545, 305–310 (2017); published online EpubMay 18 (10.1038/nature22075). [PubMed: 28489816]

21. Akers AL, Johnson E, Steinberg GK, Zabramski JM, Marchuk DA, Biallelic somatic and germline mutations in cerebral cavernous malformations (CCMs): evidence for a two-hit mechanism of CCM pathogenesis. Hum Mol Genet 18, 919–930 (2009); published online EpubMar 1 (10.1093/hmg/ddn430). [PubMed: 19088123]

22. Zawistowski JS, Stalheim L, Uhlik MT, Abell AN, Ancrile BB, Johnson GL, Marchuk DA, CCM1 and CCM2 protein interactions in cell signaling: implications for cerebral cavernous malformations pathogenesis. Hum Mol Genet 14, 2521–2531 (2005); published online EpubSep 1 (10.1093/hmg/ddi256). [PubMed: 16037064]

23. Zhou Z, Tang AT, Wong WY, Bamezai S, Goddard LM, Shenkar R, Zhou S, Yang J, Wright AC, Foley M, Arthur JS, Whitehead KJ, Awad IA, Li DY, Zheng X, Kahn ML, Cerebral cavernous malformations arise from endothelial gain of MEKK3-KLF2/4 signalling. Nature, (2016); published online EpubMar 30 (10.1038/nature17178).

24. Ridder DA, Lang MF, Salinin S, Roderer JP, Struss M, Maser-Gluth C, Schwaninger M, TAK1 in brain endothelial cells mediates fever and lethargy. J Exp Med 208, 2615–2623 (2011); published online EpubDec 19 (10.1084/jem.20110398). [PubMed: 22143887]

25. Cuttano R, Rudini N, Bravi L, Corada M, Giampietro C, Papa E, Morini MF, Maddaluno L, Baeyens N, Adams RH, Jain MK, Owens GK, Schwartz M, Lampugnani MG, Dejana E, KLF4 is a key determinant in the development and progression of cerebral cavernous malformations. EMBO Mol Med, (2015); published online EpubNov 26 (10.15252/emmm.201505433).

26. Renz M, Otten C, Faurobert E, Rudolph F, Zhu Y, Boulday G, Duchene J, Mickoleit M, Dietrich AC, Ramspacher C, Steed E, Manet-Dupe S, Benz A, Hassel D, Vermot J, Huisken J, Tournier-Lasserve E, Felbor U, Sure U, Albiges-Rizo C, Abdelilah-Seyfried S, Regulation of beta1 integrin-Klf2-mediated angiogenesis by CCM proteins. Dev Cell 32, 181–190 (2015); published online EpubJan 26 (10.1016/j.devcel.2014.12.016). [PubMed: 25625207]

27. Choi JP, Foley M, Zhou Z, Wong WY, Gokoolparsadh N, Arthur JS, Li DY, Zheng X, Micro-CT Imaging Reveals Mekk3 Heterozygosity Prevents Cerebral Cavernous Malformations in Ccm2-Deficient Mice. PLoS One 11, e0160833 (2016)10.1371/journal.pone.0160833). [PubMed: 27513872]

28. Girard R, Zeineddine HA, Orsbon C, Tan H, Moore T, Hobson N, Shenkar R, Lightle R, Shi C, Fam MD, Cao Y, Shen L, Neander AI, Rorrer A, Gallione C, Tang AT, Kahn ML, Marchuk DA, Luo ZX, Awad IA, Micro-computed tomography in murine models of cerebral cavernous malformations as a paradigm for brain disease. J Neurosci Methods 271, 14–24 (2016); published online EpubSep 15 (10.1016/j.jneumeth.2016.06.021). [PubMed: 27345427]

29. Wu GD, Chen J, Hoffmann C, Bittinger K, Chen YY, Keilbaugh SA, Bewtra M, Knights D, Walters WA, Knight R, Sinha R, Gilroy E, Gupta K, Baldassano R, Nessel L, Li H, Bushman FD, Lewis JD, Linking long-term dietary patterns with gut microbial enterotypes. Science 334, 105–108 (2011); published online EpubOct 7 (10.1126/science.1208344). [PubMed: 21885731]

30. Rothschild D, Weissbrod O, Barkan E, Kurilshikov A, Korem T, Zeevi D, Costea PI, Godneva A, Kalka IN, Bar N, Shilo S, Lador D, Vila AV, Zmora N, Pevsner-Fischer M, Israeli D, Kosower N, Malka G, Wolf BC, Avnit-Sagi T, Lotan-Pompan M, Weinberger A, Halpern Z, Carmi S, Fu J, Wijmenga C, Zhernakova A, Elinav E, Segal E, Environment dominates over host genetics in shaping human gut microbiota. Nature, (2018); published online EpubFeb 28 (10.1038/nature25973).

31. Zeineddine HA, Girard R, Saadat L, Shen L, Lightle R, Moore T, Cao Y, Hobson N, Shenkar R, Avner K, Chaudager K, Koskimaki J, Polster SP, Fam MD, Shi C, Lopez-Ramirez MA, Tang AT, Gallione C, Kahn ML, Ginsberg M, Marchuk DA, Awad IA, Phenotypic characterization of murine models of cerebral cavernous malformations. Lab Invest, (2018); published online EpubJun 26 (10.1038/s41374-018-0030-y).

32. Johansson ME, Phillipson M, Petersson J, Velcich A, Holm L, Hansson GC, The inner of the two Muc2 mucin-dependent mucus layers in colon is devoid of bacteria. Proc Natl Acad Sci U S A

105, 15064–15069 (2008); published online EpubSep 30 (10.1073/pnas.0803124105). [PubMed: 18806221]

33. Johansson ME, Gustafsson JK, Sjoberg KE, Petersson J, Holm L, Sjovall H, Hansson GC, Bacteria penetrate the inner mucus layer before inflammation in the dextran sulfate colitis model. PLoS One 5, e12238 (2010); published online EpubAug 18 (10.1371/journal.pone.0012238). [PubMed: 20805871]
34. Johansson ME, Larsson JM, Hansson GC, The two mucus layers of colon are organized by the MUC2 mucin, whereas the outer layer is a legislator of host-microbial interactions. Proc Natl Acad Sci U S A 108 Suppl 1, 4659–4665 (2011); published online EpubMar 15 (10.1073/pnas.1006451107). [PubMed: 20615996]
35. Chassaing B, Srinivasan G, Delgado MA, Young AN, Gewirtz AT, Vijay-Kumar M, Fecal lipocalin 2, a sensitive and broadly dynamic non-invasive biomarker for intestinal inflammation. PLoS One 7, e44328 (2012)10.1371/journal.pone.0044328). [PubMed: 22957064]
36. Bergstrom KS, Kissoon-Singh V, Gibson DL, Ma C, Montero M, Sham HP, Ryz N, Huang T, Velcich A, Finlay BB, Chadee K, Vallance BA, Muc2 protects against lethal infectious colitis by disassociating pathogenic and commensal bacteria from the colonic mucosa. PLoS Pathog 6, e1000902 (2010); published online EpubMay 13 (10.1371/journal.ppat.1000902). [PubMed: 20485566]
37. Birchenough GM, Nystrom EE, Johansson ME, Hansson GC, A sentinel goblet cell guards the colonic crypt by triggering Nlrp6-dependent Muc2 secretion. Science 352, 1535–1542 (2016); published online EpubJun 24 (10.1126/science.aaf7419). [PubMed: 27339979]
38. Van der Sluis M, De Koning BA, De Bruijn AC, Velcich A, Meijerink JP, Van Goudoever JB, Buller HA, Dekker J, Van Seuningen I, Renes IB, Einerhand AW, Muc2-deficient mice spontaneously develop colitis, indicating that MUC2 is critical for colonic protection. Gastroenterology 131, 117–129 (2006); published online EpubJul (10.1053/j.gastro.2006.04.020). [PubMed: 16831596]
39. Schneider MR, Dahlhoff M, Horst D, Hirschi B, Trulzsch K, Muller-Hocker J, Vogelmann R, Allgauer M, Gerhard M, Steininger S, Wolf E, Kolligs FT, A key role for E-cadherin in intestinal homeostasis and Paneth cell maturation. PLoS One 5, e14325 (2010); published online EpubDec 14 (10.1371/journal.pone.0014325). [PubMed: 21179475]
40. Draheim KM, Fisher OS, Boggon TJ, Calderwood DA, Cerebral cavernous malformation proteins at a glance. J Cell Sci 127, 701–707 (2014); published online EpubFeb 15 (10.1242/jcs.138388). [PubMed: 24481819]
41. Sonnenburg JL, Xu J, Leip DD, Chen CH, Westover BP, Weatherford J, Buhler JD, Gordon JI, Glycan foraging in vivo by an intestine-adapted bacterial symbiont. Science 307, 1955–1959 (2005); published online EpubMar 25 (10.1126/science.1109051). [PubMed: 15790854]
42. Jakobsson HE, Rodriguez-Pineiro AM, Schutte A, Ermund A, Boysen P, Bemark M, Sommer F, Backhed F, Hansson GC, Johansson ME, The composition of the gut microbiota shapes the colon mucus barrier. EMBO Rep 16, 164–177 (2015); published online EpubFeb (10.15252/embr.201439263). [PubMed: 25525071]
43. Mamantopoulos M, Ronchi F, Van Hauwermeiren F, Vieira-Silva S, Yilmaz B, Martens L, Saeys Y, Drexler SK, Yazdi AS, Raes J, Lamkanfi M, McCoy KD, Wullaert A, Nlrp6- and ASC-Dependent Inflammasomes Do Not Shape the Commensal Gut Microbiota Composition. Immunity 47, 339–348 e334 (2017); published online EpubAug 15 (10.1016/j.immuni.2017.07.011). [PubMed: 28801232]
44. Chassaing B, Koren O, Goodrich JK, Poole AC, Srinivasan S, Ley RE, Gewirtz AT, Dietary emulsifiers impact the mouse gut microbiota promoting colitis and metabolic syndrome. Nature 519, 92–96 (2015); published online EpubMar 5 (10.1038/nature14232). [PubMed: 25731162]
45. Desmet SJ, De Bosscher K, Glucocorticoid receptors: finding the middle ground. J Clin Invest 127, 1136–1145 (2017); published online EpubApr 3 (10.1172/JCI88886). [PubMed: 28319043]
46. Goodwin JE, Feng Y, Velazquez H, Sessa WC, Endothelial glucocorticoid receptor is required for protection against sepsis. Proc Natl Acad Sci U S A 110, 306–311 (2013); published online EpubJan 2 (10.1073/pnas.1210200110). [PubMed: 23248291]

47. Goodwin JE, Feng Y, Velazquez H, Zhou H, Sessa WC, Loss of the endothelial glucocorticoid receptor prevents the therapeutic protection afforded by dexamethasone after LPS. PLoS One 9, e108126 (2014)10.1371/journal.pone.0108126).

48. Das I, Png CW, Oancea I, Hasnain SZ, Lourie R, Proctor M, Eri RD, Sheng Y, Crane DI, Florin TH, McGuckin MA, Glucocorticoids alleviate intestinal ER stress by enhancing protein folding and degradation of misfolded proteins. J Exp Med 210, 1201–1216 (2013); published online EpubJun 3 (10.1084/jem.20121268). [PubMed: 23650437]

49. Becker DE, Basic and clinical pharmacology of glucocorticosteroids. Anesth Prog 60, 25–31; quiz 32 (2013); published online EpubSpring (10.2344/0003-3006-60.1.25). [PubMed: 23506281]

50. Goudreault M, D’Ambrosio LM, Kean MJ, Mullin MJ, Larsen BG, Sanchez A, Chaudhry S, Chen GI, Sicheri F, Nesvizhskii AI, Aebersold R, Raught B, Gingras AC, A PP2A phosphatase high density interaction network identifies a novel striatin-interacting phosphatase and kinase complex linked to the cerebral cavernous malformation 3 (CCM3) protein. Mol Cell Proteomics 8, 157–171 (2009); published online EpubJan (10.1074/mcp.M800266-MCP200). [PubMed: 18782753]

51. Zhang Y, Tang W, Zhang H, Niu X, Xu Y, Zhang J, Gao K, Pan W, Boggon TJ, Toomre D, Min W, Wu D, A network of interactions enables CCM3 and STK24 to coordinate UNC13D-driven vesicle exocytosis in neutrophils. Dev Cell 27, 215–226 (2013); published online EpubOct 28 (10.1016/j.devcel.2013.09.021). [PubMed: 24176643]

52. Jenny Zhou H, Qin L, Zhang H, Tang W, Ji W, He Y, Liang X, Wang Z, Yuan Q, Vortmeyer A, Toomre D, Fuh G, Yan M, Kluger MS, Wu D, Min W, Endothelial exocytosis of angiopoietin-2 resulting from CCM3 deficiency contributes to cerebral cavernous malformation. Nat Med 22, 1033–1042 (2016); published online EpubSep (10.1038/nm.4169). [PubMed: 27548575]

53. Pal S, Lant B, Yu B, Tian R, Tong J, Krieger JR, Moran MF, Gingras AC, Derry WB, CCM-3 Promotes C. elegans Germline Development by Regulating Vesicle Trafficking Cytokinesis and Polarity. Curr Biol 27, 868–876 (2017); published online EpubMar 20 (10.1016/j.cub.2017.02.028). [PubMed: 28285997]

54. McDonald DA, Shi C, Shenkar R, Stockton RA, Liu F, Ginsberg MH, Marchuk DA, Awad IA, Fasudil decreases lesion burden in a murine model of cerebral cavernous malformation disease. Stroke 43, 571–574 (2012); published online EpubFeb (10.1161/STROKEAHA.111.625467). [PubMed: 22034008]

55. Shenkar R, Shi C, Austin C, Moore T, Lightle R, Cao Y, Zhang L, Wu M, Zeineddine HA, Girard R, McDonald DA, Rorrer A, Gallione C, Pytel P, Liao JK, Marchuk DA, Awad IA, RhoA Kinase Inhibition With Fasudil Versus Simvastatin in Murine Models of Cerebral Cavernous Malformations. Stroke 48, 187–194 (2017); published online EpubJan (10.1161/STROKEAHA.116.015013). [PubMed: 27879448]

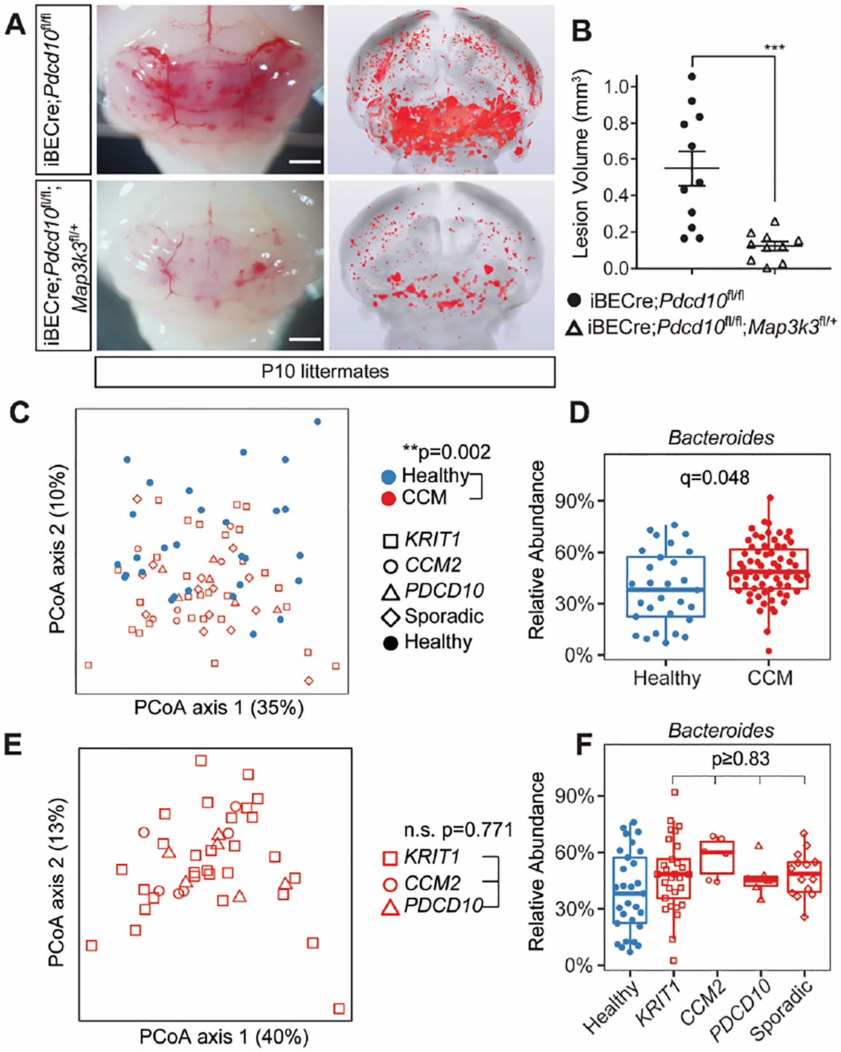

Figure 1. Comparison of PDCD10, KRIT1 and CCM2 deficiency states in mice and humans.

A, CCM lesion burden in iBECre;*Pdcd10*$^{fl/fl}$ and iBECre;*Pdcd10*$^{fl/fl}$ Map3k3$^{fl/+}$ mice at P10, assessed visually (left) and using microCT imaging (right). Scale bars 1 mm. **B**, Blinded microCT quantitation of CCM lesion burden in P10 iBECre;*Pdcd10*$^{fl/fl}$ and iBECre;*Pdcd10*$^{fl/fl}$;*Map3k3*$^{fl/+}$ littermates. n>10 animals per genotype and 4 distinct litters. **C**, Principle Coordinates Analysis (PCoA) of weighted UniFrac bacterial composition distances between the feces of individuals with familial CCM disease associated with mutations in *KRIT1*, *CCM2* and *PDCD10*, individuals with sporadic CCM disease, and age/sex-matched healthy controls. P-value compares bacterial compositions between healthy and CCM disease groups using PERMANOVA. **D**, Relative abundance boxplots of gram-negative *Bacteroides* in individuals with CCM disease and healthy controls. Significance (false discovery rate, q) determined by linear models of logit transformed relative abundances with Benjamini-Hochberg correction for multiple comparisons. **E**, PCoA of weighted UniFrac bacterial composition distances between the feces of only individuals with genotyped mutations in *KRIT1*, *CCM2* and *PDCD10*. P-values compare bacterial compositions in all groups using PERMANOVA. **F**, Relative abundance box plots of gram-negative *Bacteroides* comparing genotyped familial *KRIT1*, *CCM2*, or *PDCD10* patients with sporadic cases or healthy volunteers. Significance was determined by pairwise-testing of estimated marginal means from a linear model comparing the genetic categories of CCM disease, controlling for age and sex. All associated p-values > 0.5 and not significant (n.s.). Error bars shown as s.e.m. and significance (panel B) determined by unpaired, two-tailed Student's t-test. ***indicates $p<0.001$; n.s. indicates $p>0.05$.

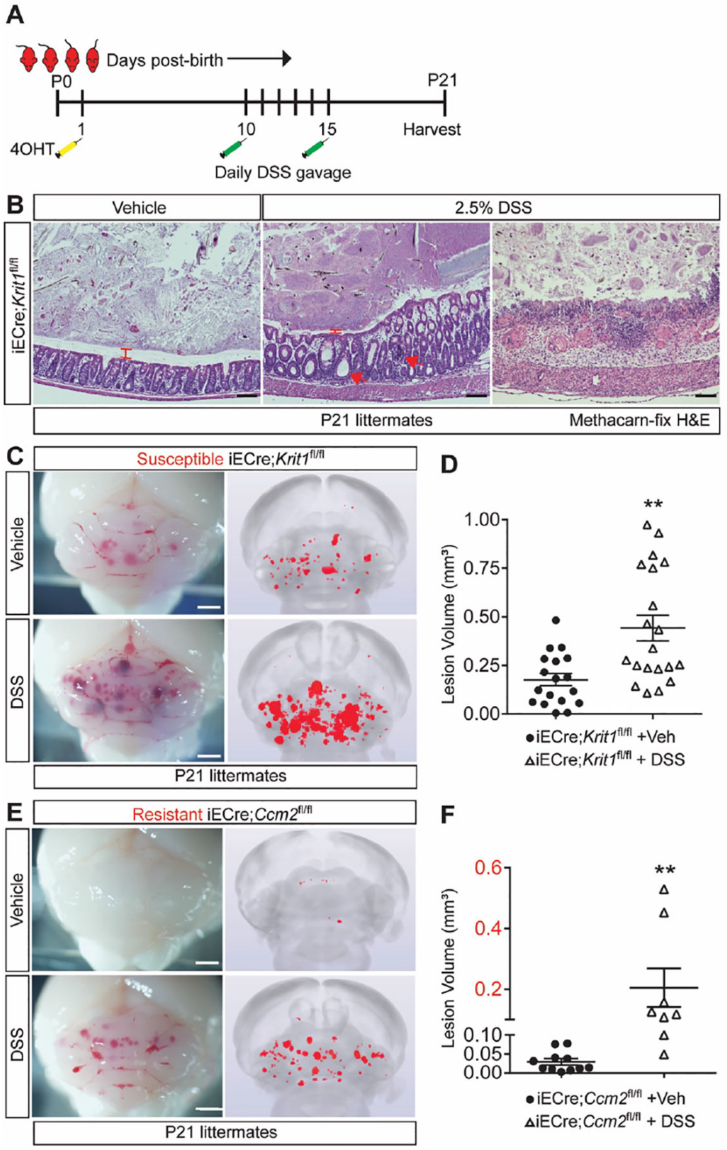

Figure 2. Effect of dextran sodium sulfate-induced colitis on CCM formation.

A, Schematic of the experimental design in which littermates receive an injection of tamoxifen one day after birth (P1), daily gavage of dextran sodium sulfate (DSS) or vehicle from P10–15, and tissue harvest at P21. **B**, DSS-treated iECre;*Krit1*$^{fl/fl}$ mice exhibit colitis of varying severity associated with thinned mucus layer (red bracket), crypt dilation and abscesses (red arrows) and an inflamed (middle) or entirely eroded (right) epithelium. Scale bars 100 µm. Results representative of n>3 animals per treatment group. **C**, CCM lesion burden in susceptible iECre;*Krit1*$^{fl/fl}$ mice was measured following DSS or vehicle exposure assessed visually (left panels) and using microCT imaging (right panels). Scale bars 1 mm. **D**, Blinded microCT quantitation of CCM lesion burden in P21 iECre;*Krit1*$^{fl/fl}$ littermates following gavage with vehicle or DSS. n>18 per treatment group and 8 distinct litters.. **E**, CCMs form in resistant iECre;*Ccm2*$^{fl/fl}$ mice following DSS exposure. CCMs were assessed visually (left panels) and using microCT imaging (right panels). Scale bars 1 mm. **F**, Blinded microCT quantitation of CCM lesion burden in resistant P21 iECre;*Ccm2*$^{fl/fl}$ littermates following gavage with vehicle or DSS. n≥8 per treatment group and 4 distinct litters. Error bars shown as s.e.m. and significance determined by unpaired, two-tailed Welch's t-test (panel D) or unpaired, two-tailed Student's t-test (panel F). **indicates $p<0.01$

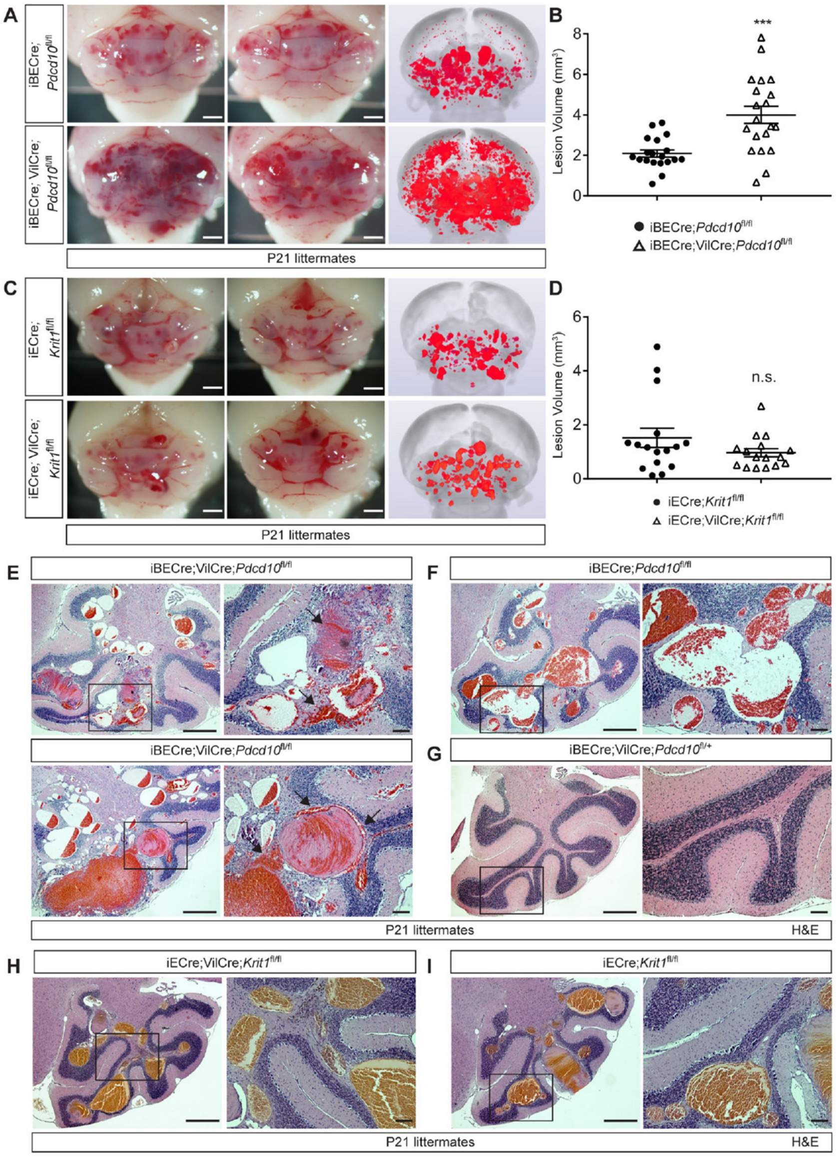

Figure 3. Effect of brain endothelial and gut epithelial loss of PDCD10 or KRIT1 on CCM formation.

A, CCM formation in iBECre;*Pdcd10*$^{\text{fl/fl}}$ and iBECre;VilCre;*Pdcd10*$^{\text{fl/fl}}$ littermates assessed visually (left and middle panels) and using microCT imaging (right panels). Scale bars 1 mm. **B**, Blinded microCT quantitation of CCM lesion burden in P21 iBECre;*Pdcd10*$^{\text{fl/fl}}$ and iBECre;VilCre;*Pdcd10*$^{\text{fl/fl}}$ littermates. n≥19 animals per genotype and 10 distinct litters. **C**, CCM formation in iECre;*Krit1*$^{\text{fl/fl}}$ and iECre;VilCre;*Krit1*$^{\text{fl/fl}}$ littermates was assessed visually (left and middle panels) and using microCT imaging (right panels). Scale bars 1mm. **D**, Blinded microCT quantitation of CCM lesion burden in P21 iECre;*Krit1*$^{\text{fl/fl}}$ and iECre;VilCre;*Krit1*$^{\text{fl/fl}}$ littermates. n≥16 animals per genotype and 7 distinct litters. **E-G**, H&E staining of hindbrain sections from P21 iBECre;VilCre;*Pdcd10*$^{\text{fl/fl}}$, iBECre;*Pdcd10*$^{\text{fl/fl}}$, and iBECre;VilCre;*Pdcd10*$^{\text{fl/+}}$ littermates. Arrows indicate extravascular hemorrhage that was observed in iBECre;VilCre;*Pdcd10*$^{\text{fl/fl}}$ animals. Boxes in left images denote area of magnified image on the right. Scale bars 500 μm (left images) and 100 μm (right images**).**

H-I, H&E staining of hindbrain sections from P21 iECre;Krit1$^{fl/fl}$ and iECre;VilCre;Krit1$^{fl/fl}$ littermates. Boxes in left images denote area of magnified image on the right. Scale bars 500 µm (left images) and 100 µm (right images). Results representative of n≥3 animals per genotype and four distinct litters. Error bars shown as s.e.m. and significance determined by unpaired, two-tailed Welch’s t-test. ***indicates $p<0.001$; n.s. indicates $p>0.05$.

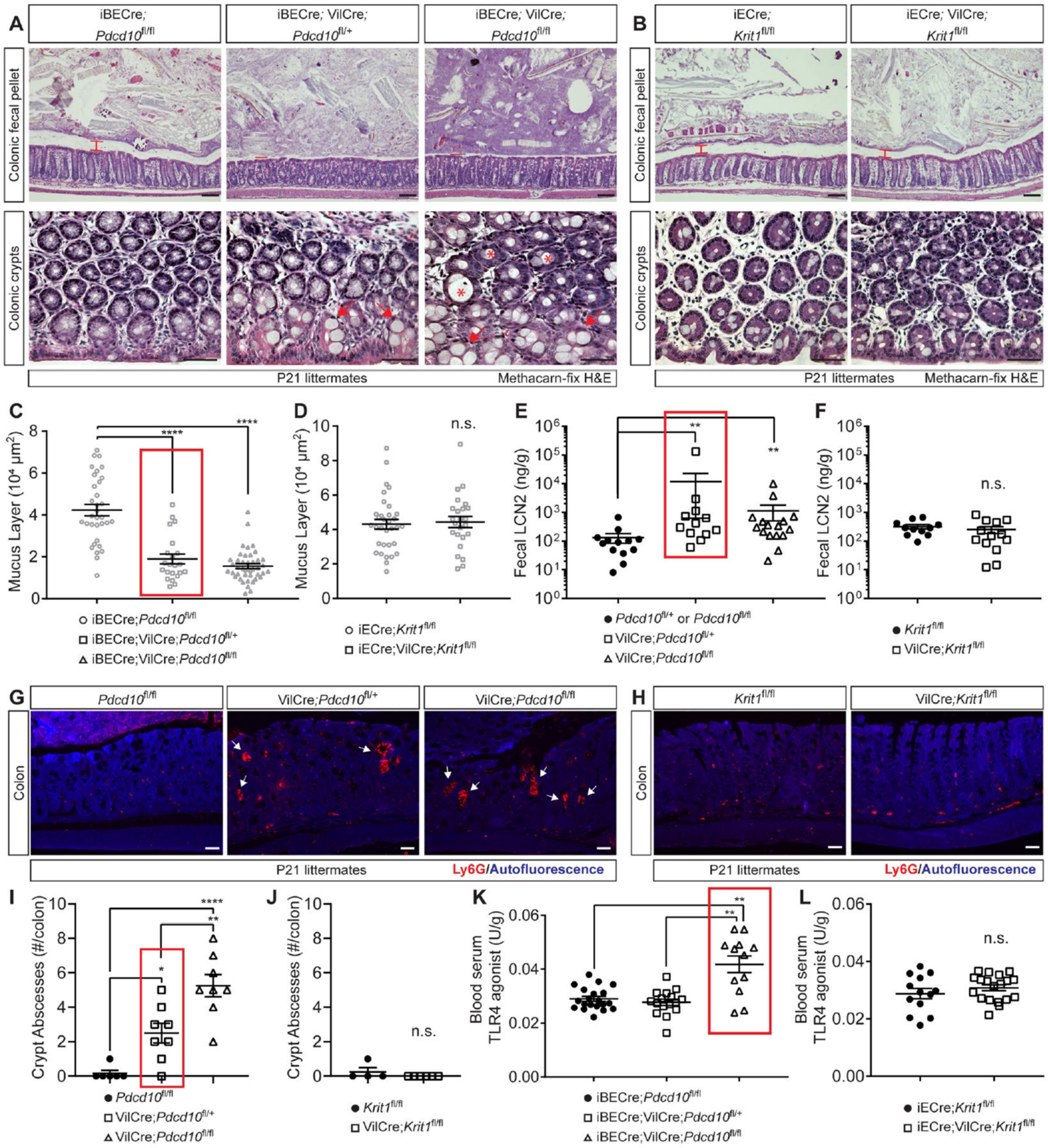

Figure 4. Gut barrier and blood TLR4 ligand following gut epithelial loss of PDCD10 or KRIT1.

A-B, H&E histology of methacarn-fixed colons from iBECre;*Pdcd10*$^{fl/fl}$, iBECre;VilCre;*Pdcd10*$^{fl/+}$, and iBECre;VilCre;*Pdcd10*$^{fl/fl}$ animals (A) or iECre;*Krit1*$^{fl/fl}$ and iECre;VilCre;*Krit1*$^{fl/fl}$ animals (B) at P21. Low magnification images of the colonic fecal pellet (top) and higher magnification images of the colonic crypts (bottom). The brains of these animals with CCM lesions are shown in Figure 3. Brackets denote the thickness of the mucus layer. Arrows indicate goblet cells. Asterisks highlight colonic crypts. Scale bars 100 μm (top panels) and 50 μm (bottom panels). Results are representative of n≥16 animals per genotype and at least 7 distinct litters. **C-D**, Quantitation of colonic mucus layer from the indicated H&E stained, methacarn-fixed, tissue sections in A and B. Each point represents measurements around one fecal pellet, n≥16 animals per genotype and at least 7 distinct litters. **E**, Fecal lipocalin-2 (LCN2) concentration measured by ELISA in VilCre;*Pdcd10*$^{fl/fl}$, VilCre;*Pdcd10*$^{fl/+}$, or littermate controls (*Pdcd10*$^{fl/+ \text{ or } fl/fl}$). n≥12 animals per genotype from

4 distinct litters. **F**, Fecal LCN2 concentration measured by ELISA in VilCre;*Krit1*$^{fl/fl}$ and littermate *Krit1*$^{fl/fl}$ animals. n≥11 animals per genotype and 3 distinct litters. **G-H**, Immunostaining for the neutrophil marker Ly6G is shown for P21 colons from *Pdcd10*$^{fl/fl}$, VilCre;*Pdcd10*$^{fl/+}$, VilCre;*Pdcd10*$^{fl/fl}$ littermates and *Krit1*$^{fl/fl}$, VilCre;*Krit1*$^{fl/fl}$ littermates. Scale bars 50 μm. **I-J**, Quantification of Ly6G-positive crypt abscesses per colonic section analyzed. Each point represents a distinct animal. Results are representative of n≥ 4 animals per genotype and at least 3 distinct litters. **K-L**, TLR4 agonist activity detected in the blood of VilCre;*Pdcd10*$^{fl/fl}$ animals and VilCre;*Krit1*$^{fl/fl}$ animals. n≥13 animals per genotype and at least 7 distinct litters. Error bars shown as s.e.m. and significance determined by Kruskall-Wallis one-way ANOVA with Dunn’s correction for multiple comparisons (panels C, E, I) or unpaired, two-tailed Student’s t-test (panels D, F, J). ****indicates $p<0.0001$; **indicates $p<0.01$; n.s. indicates $p>0.05$.

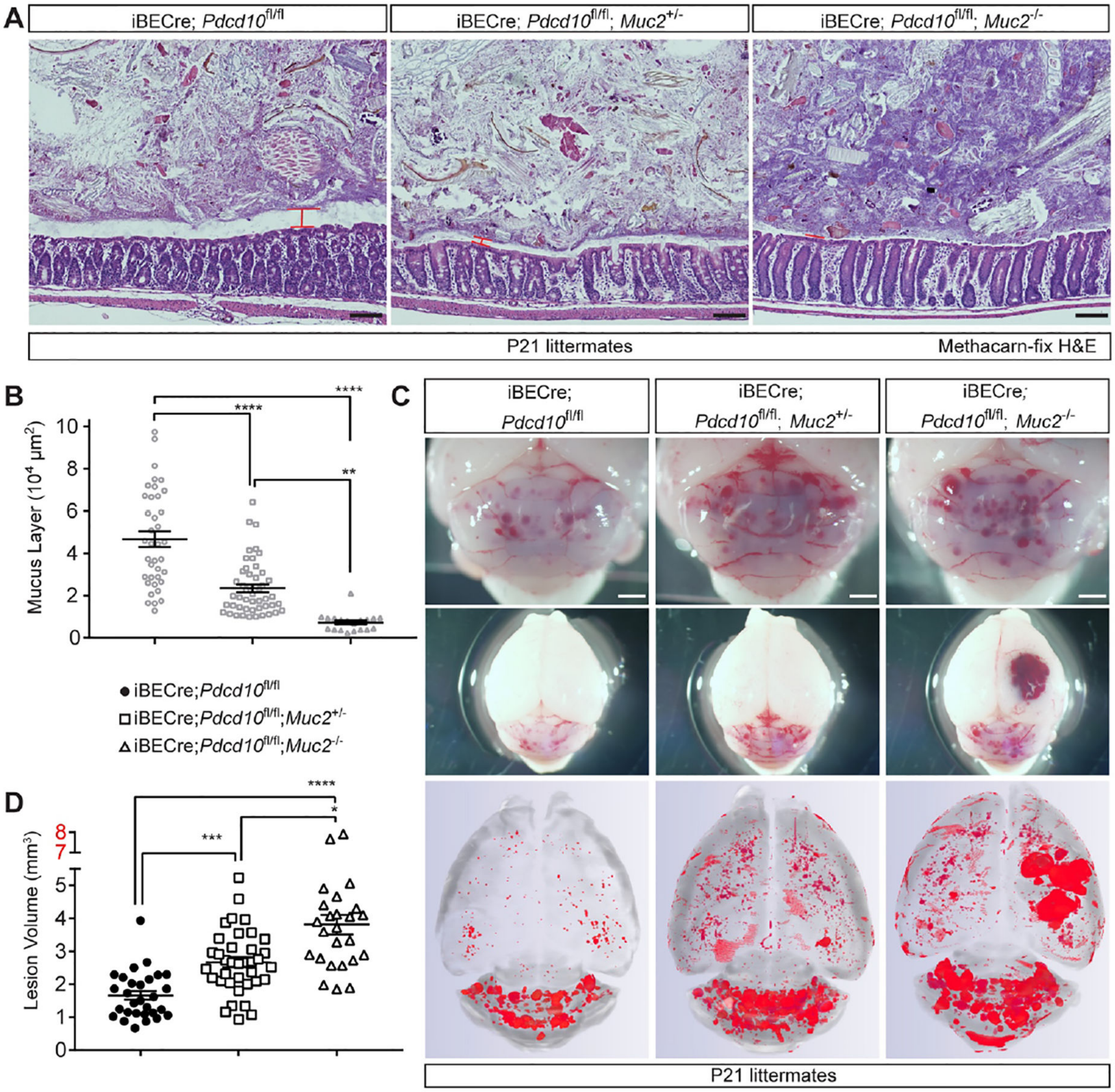

Figure 5. Relationship of the colonic mucus barrier and CCM formation.

A, H&E staining of methacarn fixed colon samples from iBECre;*Pdcd10*$^{fl/fl}$, iBECre;*Pdcd10*$^{fl/fl}$*;Muc2*$^{+/-}$, and iBECre;*Pdcd10*$^{fl/fl}$*;Muc2*$^{-/-}$ animals. The mucus barrier is indicated with brackets. Scale bars 100 μm. **B**, Quantitation of the area of the mucus layers shown in (A). Each point represents measurement around one fecal pellet. n≥10 animals per genotype and 9 distinct litters. **C**, CCM formation in representative P21 iBECre;*Pdcd10*$^{fl/fl}$, iBECre;*Pdcd10*$^{fl/fl}$*;Muc2*$^{+/-}$, and iBECre;*Pdcd10*$^{fl/fl}$*;Muc2*$^{-/-}$ animals is shown visually in the hindbrain (top), hindbrain and forebrain (middle) and with microCT imaging (bottom). Scale bars 1 mm. **D**, Blinded microCT quantification of CCM lesion volumes in P21 iBECre;*Pdcd10*$^{fl/fl}$, iBECre;*Pdcd10*$^{fl/fl}$*;Muc2*$^{+/-}$, and iBECre;*Pdcd10*$^{fl/fl}$*;Muc2*$^{-/-}$ littermates. n≥25 animals per genotype and 17 distinct litters. Error bars shown as s.e.m. and significance determined by Kruskall-Wallis one-way ANOVA with Dunn’s correction for multiple comparisons (panels B and D). ****indicates $p<0.0001$; ***indicates $p<0.001$;**indicates $p<0.01$; *indicates $p<0.05$

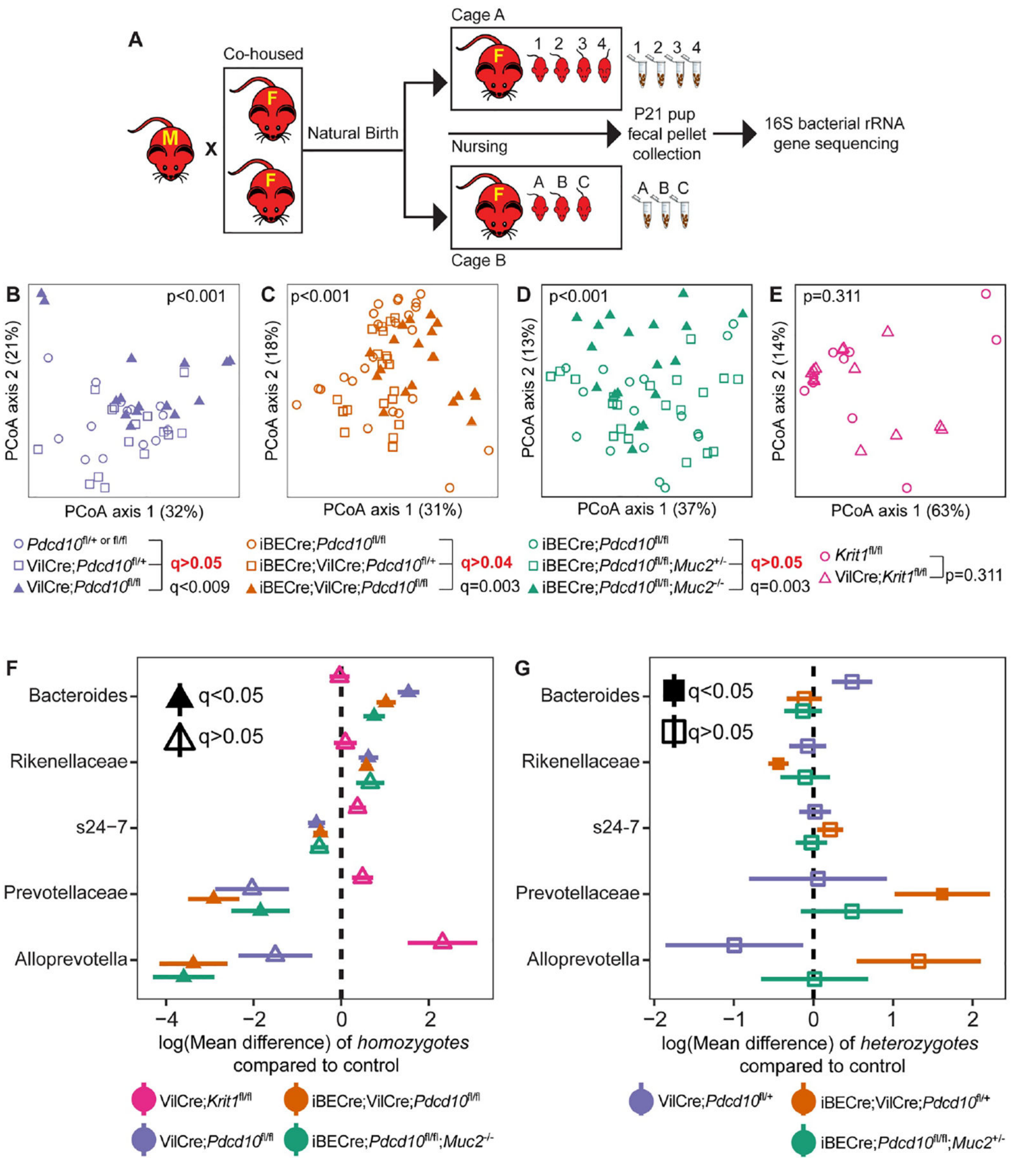

Figure 6. Analysis of the gut microbiome following loss of gut epithelial PDCD10 or MUC2.

A, Experimental design in which females were mated, individually housed prior to natural delivery of pups, and fecal pellets collected from each pup at P21 prior to weaning for 16S rRNA bacterial gene sequencing. **B-E**, Principle Coordinates Analysis (PCoA) of weighted UniFrac bacterial composition distances from the feces of the indicated animals. Each box shows analysis of littermate animals while accounting for caging differences. P-values compare bacterial compositions in the indicated groups using PERMANOVA also considering individual cage differences and corrected for multiple comparisons using the Bonferroni method. (B-D). n≥10 animals per genotype and at least four distinct cages/litters. Overall p-values comparing homozygous animals to wildtype or heterozygous controls are shown in plot, as well as the pairwise comparisons (q-values) in legend. **F**, Mean difference of logit transformed relative abundance of the indicated bacteria taxa estimated with linear mixed effects models in VilCre;*Krit1*$^{fl/fl}$, VilCre;*Pdcd10*$^{fl/fl}$, iBECre;VilCre;*Pdcd10*$^{fl/fl}$, and iBECre;*Pdcd10*$^{fl/fl}$;*Muc2*$^{-/-}$ animals compared to their respective VilCre-negative or *Muc2*$^{+/+}$ littermate controls. **G**, Mean difference of logit transformed relative abundance of the indicated bacteria taxa estimated with linear mixed effects models in VilCre;*Pdcd10*$^{fl/+}$, iBECre;VilCre;*Pdcd10*$^{fl/+}$, and iBECre;*Pdcd10*$^{fl/fl}$;*Muc2*$^{+/-}$ animals compared to their respective VilCre-negative or *Muc2*$^{+/+}$ littermate controls. Significance (false discovery rate, q) determined by linear mixed effects models with Benjamini-Hochberg correction for multiple comparisons.

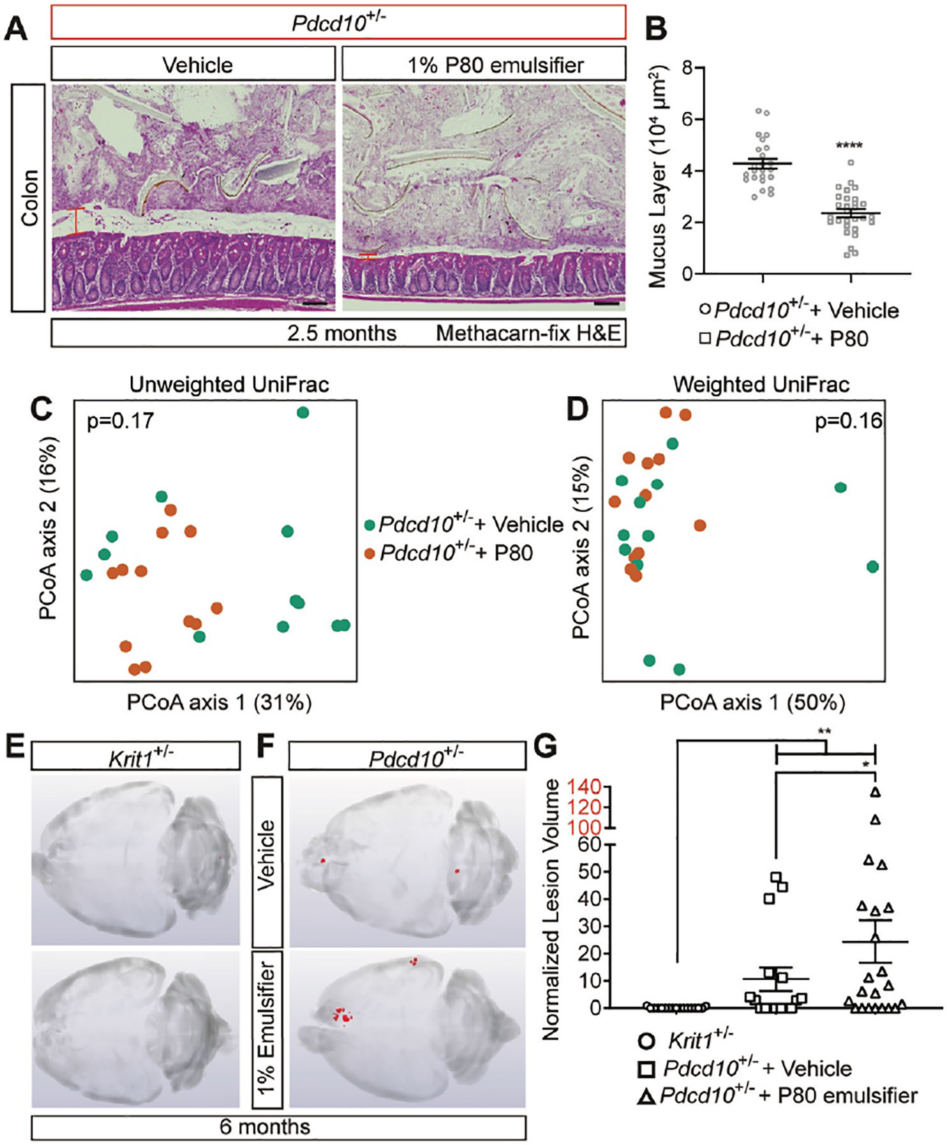

Figure 7. Effects of chronic P80 dietary emulsifier intake on the colonic mucosal barrier and CCM formation.

A, H&E staining of methacarn fixed colon samples from vehicle and *Pdcd10*$^{+/-}$ animals administered 1% P80 in drinking water for two weeks. The mucus barrier is indicated with brackets. Scale bars 100 μm. **B**, Quantitation of the area of the mucus layers shown in (A). Each point represents measurement around one fecal pellet. n=7 animals per genotype. **C-D**, Principle Coordinates Analysis (PCoA) of unweighted and weighted UniFrac bacterial composition distances from the feces of the indicated animals administered 1% P80 for 4 months is shown. P-values compare bacterial compositions in the indicated groups using PERMANOVA also considering individual cage differences and corrected for multiple comparisons using the Bonferroni method.. n=12 animals per genotype and five distinct cages per treatment. **E-G**, Spontaneous CCM formation was analyzed using microCT imaging (E, F) and lesion volume measurement normalized to total brain volume (G) in animals of the indicated genotypes administered 1% P80 for 4 months. n≥16 animals per treatment group. Error bars shown as s.e.m. and significance determined by Kruskall-Wallis one-way ANOVA with Dunn’s correction for multiple comparisons (B and D) or Mann-Whitney non-parametric U-test (G). ****indicates $p<0.0001$; **indicates $p<0.01$; *indicates $p<0.05$.

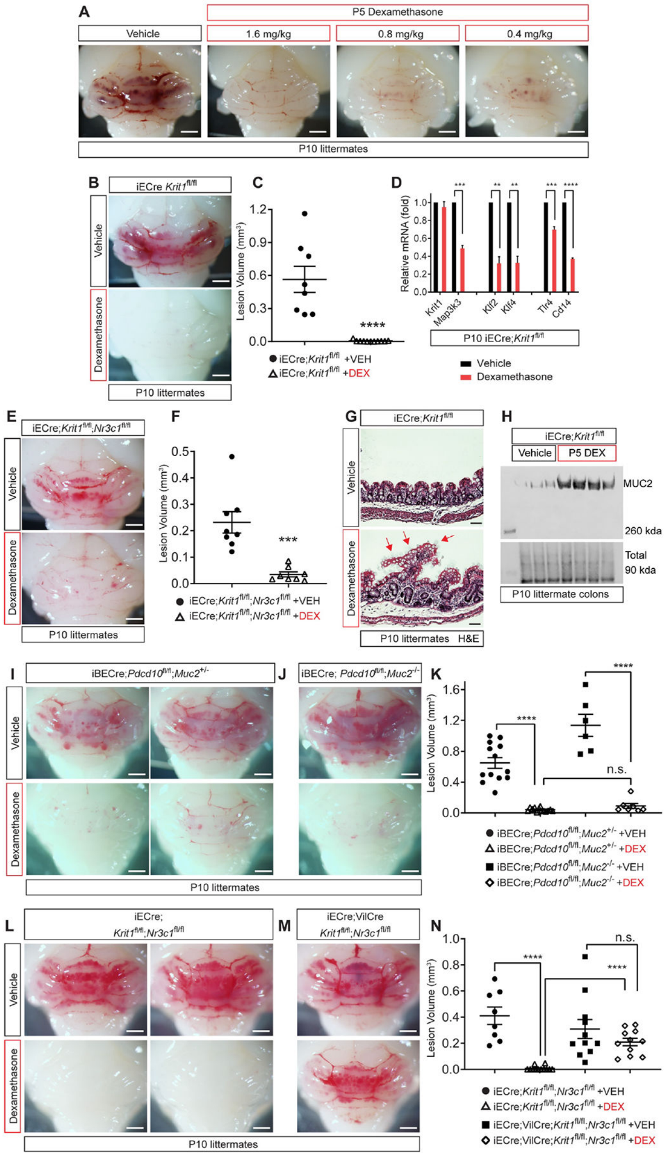

Figure 8. Dexamethasone therapy highlights a gut-brain CCM axis.

A, Visual assessment of CCM formation in ten-day old (P10) iECre;*Krit1*$^{fl/fl}$ littermates treated at P5 with vehicle or the indicated doses of dexamethasone. 0.8 mg/kg dose was used for all following experiments. Scale bars 1 mm. Images are representative of n≥3 animals per treatment group from at least 2 distinct litters. **B**, Visual assessment of CCM formation in iECre;*Krit1*$^{fl/fl}$ littermates treated with vehicle or dexamethasone. Scale bars 1 mm. **C**, Blinded microCT quantitation of CCM lesion burden in P10 iCre;*Krit1*$^{fl/fl}$ littermates treated with vehicle or dexamethasone. n≥8 animals per treatment group and 3 distinct litters. **D**, Relative amounts of *Krit1, Map3k3, Klf2*, *Klf4, Tlr4*, and *Cd14* expression in cerebellar endothelial cells freshly isolated from P10 iECre;*Krit1*$^{fl/fl}$ littermates treated with P5 vehicle or dexamethasone. n≥4 animals per treatment group and 3 distinct litters. **E**, Visual assessment of CCM formation in iECre;*Krit1*$^{fl/fl}$;*Nr3c1*$^{fl/fl}$ littermates treated with vehicle or dexamethasone. Scale bars 1 mm. Results are representative of n≥5 animals per group and five independent experiments. **F**, Blinded microCT quantitation of CCM lesion burden in P10 iECre;*Krit1*$^{fl/fl}$;*Nr3c1*$^{fl/fl}$ littermates treated with vehicle or dexamethasone. n≥8 animals per treatment group and 3 distinct litters. **G**, H&E staining of P10 colon sections from iECre;*Krit1*$^{fl/fl}$ littermates treated with P5 vehicle or dexamethasone. Note the goblet cells in the dexamethasone treated colon (arrows). Scale bars 50 μm. **H**, Immunoblot analysis of MUC2-expression in P10 colons from iECre;*Krit1*$^{fl/fl}$ littermates treated with P5 vehicle or dexamethasone (top, anti-MUC2). Total protein loading detected using REVERT™ is shown below. Molecular weight markers (kDa) on left. Each lane is whole colonic lysate from one distinct animal. Results are representative of n≥5 animals per group and two distinct litters. **I-J**, Visual assessment of CCM formation in iBECre;*Pdcd10*$^{fl/fl}$;*Muc2*$^{+/-}$ (I) and iBECre;*Pdcd10*$^{fl/fl}$;*Muc2*$^{-/-}$ (J) animals treated with P5 vehicle or dexamethasone. Scale bars 1 mm. **K**, Blinded microCT quantitation of CCM lesion burden in P10 iBECre;*Pdcd10*$^{fl/fl}$;*Muc2*$^{+/-}$ and iBECre;*Pdcd10*$^{fl/fl}$;*Muc2*$^{-/-}$ littermates treated with vehicle or dexamethasone. n≥6 animals per treatment group and ≥3 distinct litters. **L-M**, Visual assessment of CCM formation in iECre;*Krit1*$^{fl/fl}$;*Nr3c1*$^{fl/fl}$ (L) and iECre;VilCre;*Krit1*$^{fl/fl}$;*Nr3c1*$^{fl/fl}$ (M) littermates at P10 after treatment with P5 vehicle or dexamethasone.. Scale bars 1 mm. **N**, Blinded microCT quantitation of CCM lesion burden in P10 iECre;*Krit1*$^{fl/fl}$;*Nr3c1*$^{fl/fl}$ and iECre;VilCre;*Krit1*$^{fl/fl}$;*Nr3c1*$^{fl/fl}$ littermates treated with vehicle or dexamethasone. n≥8 animals per treatment group and 3 distinct litters. Error bars shown as s.e.m. and significance determined by unpaired, two-tailed Student's t-test. ****indicates p<0.0001; ***indicated p<0.001; **indicates p<0.01.